ASTHMA

Steroid-resistant human inflammatory ILC2s are marked by CD45RO and elevated in type 2 respiratory diseases

Esmee K. van der Ploeg[1,2]*, Korneliusz Golebski[3,4]*, Menno van Nimwegen[1], Joannah R. Fergusson[3], Balthasar A. Heesters[3], Itziar Martinez-Gonzalez[3], Chantal M. A. Kradolfer[3], Sophie van Tol[3], Brendon P. Scicluna[5,6], Marjolein J. W. de Bruijn[1], Geertje M. de Boer[1,7], Gerdien A. Tramper-Stranders[8,9], Gert-Jan Braunstahl[1,7], Wilfred F. J. van IJcken[2,10], A. Paul Nagtegaal[11], Cornelis M. van Drunen[12], Wytske J. Fokkens[12], Danny Huylebroeck[2], Hergen Spits[3†], Rudi W. Hendriks[1], Ralph Stadhouders[1,2†‡], Suzanne M. Bal[1,3‡]

Group 2 innate lymphoid cells (ILC2s) orchestrate protective type 2 immunity and have been implicated in various immune disorders. In the mouse, circulatory inflammatory ILC2s (iILC2s) were identified as a major source of type 2 cytokines. The human equivalent of the iILC2 subset remains unknown. Here, we identify a human inflammatory ILC2 population that resides in inflamed mucosal tissue and is specifically marked by surface CD45RO expression. CD45RO$^+$ ILC2s are derived from resting CD45RA$^+$ ILC2s upon activation by epithelial alarmins such as IL-33 and TSLP, which is tightly linked to STAT5 activation and up-regulation of the IRF4/BATF transcription factors. Transcriptome analysis reveals marked similarities between human CD45RO$^+$ ILC2s and mouse iILC2s. Frequencies of CD45RO$^+$ inflammatory ILC2 are increased in inflamed mucosal tissue and in the circulation of patients with chronic rhinosinusitis or asthma, correlating with disease severity and resistance to corticosteroid therapy. CD45RA-to-CD45RO ILC2 conversion is suppressed by corticosteroids via induction of differentiation toward an immunomodulatory ILC2 phenotype characterized by low type 2 cytokine and high amphiregulin expression. Once converted, however, CD45RO$^+$ ILC2s are resistant to corticosteroids, which is associated with metabolic reprogramming resulting in the activation of detoxification pathways. Our combined data identify CD45RO$^+$ inflammatory ILC2s as a human analog of mouse iILC2s linked to severe type 2 inflammatory disease and therapy resistance.

INTRODUCTION

Type 2 immunity confers host defense against parasites, neutralizes toxins, and organizes tissue repair. However, type 2 immune responses can also fuel common immunopathologies such as allergies, chronic rhinosinusitis, and asthma (*1*). Hallmarks of type 2 immunity at mucosal barrier sites include eosinophilic inflammation, immunoglobulin E (IgE) secretion by plasma cells, and tissue remodeling. These processes are orchestrated by the signature cytokines interleukin-4 (IL-4), IL-5, IL-9, and IL-13, which are produced by both innate and adaptive immune cells (*1*).

Group 2 innate lymphoid cells (ILC2s) are major producers of type 2 cytokines that are characterized by high levels of the GATA3 transcription factor, analogous to CD4$^+$ T helper 2 (T_H2) cells of the adaptive immune system (*2*). In mouse models, ILC2s play a central role in mounting type 2 immune responses against helminths and in maintaining tissue homeostasis. Moreover, ILC2s are key inflammatory cytokine producers in allergic airway inflammation (*3*, *4*). ILC2s mostly reside in mucosal and barrier tissues (*4*, *5*), where they are able to respond to activating environmental signals, including cytokines, lipid mediators, and neuropeptides (*3*, *6*, *7*). Alarmins produced by activated or damaged epithelial cells, including IL-25, IL-33, and thymic stromal lymphopoietin (TSLP), induce ILC2s to promote inflammation by producing copious amounts of IL-5 and IL-13 (*1*). In addition, IL-33 can induce the expression of the growth factor amphiregulin by ILC2s to orchestrate epithelial tissue repair after influenza infection or intestinal injury (*8*, *9*).

ILC2s can adopt tissue- and stimulus-dependent phenotypes (*10*–*14*), including the acquisition of cytokine-producing capacities associated with plasticity toward other ILC subsets (*15*). Mouse ILC2s are not strictly a tissue-resident population, as they can enter the circulation and traffic between tissues under inflammatory conditions (*16*–*18*). Migratory ILC2s were also detected in lymph nodes under steady-state conditions (*19*). Mouse models of type 2 immunity identified two subsets of ILC2s: natural ILC2s (nILC2s) that are tissue resident and inflammatory ILC2s (iILC2s) with the capacity to migrate (*14*, *18*, *20*–*22*). Initially, mouse iILC2s were characterized by high levels of the killer cell lectin-like receptor KLRG1 and preferential responsiveness to IL-25 instead of IL-33 (*14*), but a recent

[1]Department of Pulmonary Medicine, Erasmus MC, Rotterdam, Netherlands. [2]Department of Cell Biology, Erasmus MC, Rotterdam, Netherlands. [3]Department of Experimental Immunology, Amsterdam University Medical Centers, University of Amsterdam, Amsterdam, Netherlands. [4]Department of Respiratory Medicine, Amsterdam University Medical Centers, University of Amsterdam, Amsterdam, Netherlands. [5]Center of Experimental and Molecular Medicine, Amsterdam University Medical Centers, University of Amsterdam, Amsterdam, Netherlands. [6]Department of Clinical Epidemiology and Biostatistics, Amsterdam University Medical Centers, University of Amsterdam, Amsterdam, Netherlands. [7]Department of Respiratory Medicine, Franciscus Gasthuis and Vlietland, Rotterdam, Netherlands. [8]Department of Pediatric Medicine, Franciscus Gasthuis and Vlietland, Rotterdam, Netherlands. [9]Department of Neonatology, Sophia Children's Hospital, Erasmus MC, Rotterdam, Netherlands. [10]Center for Biomics, Erasmus MC, Rotterdam, Netherlands. [11]Department of Otorhinolaryngology and Head and Neck Surgery, Erasmus MC, Rotterdam, Netherlands. [12]Department of Otorhinolaryngology, Amsterdam University Medical Centers, University of Amsterdam, Amsterdam, Netherlands.
*These authors contributed equally to this work.
†Corresponding author. Email: r.stadhouders@erasmusmc.nl (R.S.); hergen.spits@amsterdamumc.nl (H.S.)
‡These authors contributed equally to this work.

study demonstrated that IL-33 can also promote iILC2 generation (*21*). Unlike the nILC2s that already reside in tissues under steady-state conditions, iILC2s (i) are generated upon induction of type 2 inflammation or exposure to epithelial alarmins, (ii) express low levels of the metabolic enzyme arginase, and (iii) have the capacity to enter the circulation (*14*, *20*–*22*). In mice, these migratory iILC2s represent a major early source of type 2 cytokines and subsequent host protection against helminth infections (*18*, *20*). The activator protein–1 (AP-1) family transcription factor BATF was recently identified as an essential regulator of mouse iILC2, but not nILC2, function (*20*). The origin and abundance of migratory iILC2s appear to strongly depend on the nature of the stimulus and the timing during inflammation (*18*, *22*). In vitro conversion between nILC2 and iILC2 phenotypes has been reported (*14*, *23*), as well as inter-organ trafficking of iILC2s to parasite-infected lungs and extrusion of alarmin-activated local ILC2s into the circulation (*18*, *22*).

Although ILC2 activation has been extensively studied in mouse models of type 2 inflammation, our understanding of the mechanisms that control human ILC2 activity and phenotypic heterogeneity under inflammatory conditions is limited. Human ILC2s develop from multipotent ILC precursors through a committed KLRG1$^+$ ILC2 progenitor stage and can be found in the circulation (*24*–*26*). Much like their murine counterparts, human ILC2 populations are heterogeneous and exhibit phenotypic plasticity (*15*). However, how circulating human ILC2s relate to those found within tissues is poorly understood. Moreover, a human analog of the mouse iILC2, which has the capacity to circulate and is strongly associated with tissue inflammation, has not yet been identified.

Despite these limitations in our knowledge of human ILC2 biology, the activation of ILC2s has been linked to type 2 immune disorders such as chronic rhinosinusitis with nasal polyps (CRSwNP) and allergic asthma (*27*, *28*). ILC2s have become a major focus of research on type 2 inflammatory disease, with several studies suggesting that the frequency and phenotype of circulating or tissue ILC2s are predictive of disease severity or therapy response [as reviewed for asthma in (*28*)]. In this context, ILC2s have recently been implicated in mediating resistance to immunosuppression by corticosteroids (*29*–*35*), a mainstay treatment for CRSwNP and asthma to which a substantial number of patients fail to adequately respond (*36*–*38*). However, such studies often reported conflicting results, still casting doubt on the precise role of ILC2s in these immunopathologies and therapy resistance.

We set out to characterize human ILC2 populations in peripheral blood (PB) and tissue samples to couple functional ILC2 heterogeneity to type 2 inflammatory disease. We identify inflammatory CD45RO$^+$ ILC2s in the circulation and inflamed mucosal tissue of patients suffering from type 2 immunopathologies and present evidence that these cells are derived from resting CD45RA$^+$ ILC2s upon exposure to epithelial alarmins. Our combined data make a compelling case for CD45RO$^+$ ILC2s to represent the human equivalent of the circulatory iILC2s described in mouse models of type 2 inflammation. Inflammatory CD45RO$^+$ ILC2s specifically confer resistance to corticosteroids, are elevated in PB samples of patients with asthma and CRSwNP, and correlate with disease severity as well as therapy resistance.

RESULTS

CD45RO expression identifies activated ILC2s from inflamed human mucosal tissue

To characterize the transcriptional differences between resting ILC2s and activated ILC2s from an inflamed microenvironment, we performed microarray gene expression analysis on ILC2s isolated from PB of healthy control (HC) individuals and from nasal polyp (NP) tissue surgically removed from patients with CRSwNP. We identified >18,000 similarly expressed genes between PB and NP ILC2s, including core ILC2 identity genes such as *GATA3*, *RORA*, *IL7R*, and *PTGDR2* (encoding CRTH2) (Fig. 1, A to D). A total of 1279 genes were differentially expressed (adjusted $P < 0.05$), of which 286 genes were up-regulated in NP ILC2s (Fig. 1A, fig. S1A, and table S1). Pathway analysis of these 286 genes revealed a robust enrichment for genes involved in cytokine signaling and leukocyte activation (Fig. 1, B and C). NP ILC2s displayed increased expression of genes associated with ILC2 activation, including *IL1RL1* (encoding the IL-33 receptor), *IL2RA*, *ICOS*, *AREG*, *CSF1*, and *IL13*, and lipid metabolism genes such as *PTGDR* (DP1) (Fig. 1D and fig. S1B) (*39*, *40*). In addition, several genes implicated in tissue residency were differentially expressed in NP ILC2s, e.g., up-regulation of *NR4A1* and down-regulation of *S1PR1* and *ITGB2*. NP ILC2s did not exhibit overt signs of plasticity toward an ILC1 or ILC3 phenotype, as expression levels of *IFNG*, *IL17A*, *IL22*, *TBX21*, and *RORC* remained low (Fig. 1D and fig. S1B).

We next compared the inflammatory NP ILC2 population with resting PB ILC2s at the protein level using flow cytometry. Given the enrichment for differentially expressed genes associated with T($_H$2) cell activation (Fig. 1, B to D, and fig. S1B), we stained for various well-known T cell activation markers. Consistent with our gene expression analysis, NP ILC2s exhibited an activated phenotype compared with PB ILC2s, showing increased surface expression of CD69 and ICOS (Fig. 1E). We observed elevated expression of the chemokine receptor CCR10, which is present on ILC2s from asthmatic patients (*41*), as well as decreased levels of the lymph node homing receptor CD62L (Fig. 1E). Culturing PB and NP ILC2s in the presence of IL-2 revealed that the NP ILC2 population was also functionally more activated, because only these cells produced substantial amounts of IL-5 and IL-13 (Fig. 1F).

CD45 is a receptor tyrosine phosphatase found on the surface of most blood cell types, including ILCs and T cells (*42*). Whereas naive T cells express the CD45RA splicing isoform, activated and memory T cells exclusively express CD45RO. Resting PB ILC2s were mostly CD45RA$^+$, and NP ILC2s contained a large fraction of CD45RO$^+$ cells, analogous to the CD45 isoform switch that accompanies T cell activation (Fig. 1, G and H, and fig. S1C). CD45RO$^+$ ILC2s were essentially negative for surface CD117 (the c-KIT receptor) (Fig. 1I), indicating decreased potential for plasticity (*43*, *44*). To exclude the possibility that the activated phenotype of NP ILC2s simply reflects their location, we determined the proportions of CD45RA$^+$ and CD45RO$^+$ ILC2s in noninflamed nasal turbinate (TB) tissue. TB ILC2s were virtually all CD45RA$^+$, demonstrating that the activated CD45RO$^+$ ILC2 phenotype does not simply reflect their location in the nasal mucosal microenvironment, but instead is linked to inflammation (Fig. 1, G and H). We consistently detected an increased proportion (~20%) of CD45RO$^+$ ILC2s in PB samples from patients with CRSwNP compared with HCs (Fig. 1, G and H). Sorted CD45RO$^+$ NP ILC2s showed higher type 2 cytokine mRNA expression levels as compared with CD45RA$^+$ NP ILC2s (Fig. 1J and fig. S1D), indicating that CD45 isoform expression on ILC2s is linked to their activation status in tissues.

Cytokine stimuli trigger differentiation of resting CD45RA$^+$ ILC2s into inflammatory CD45RO$^+$ ILC2s

The identification of CD45RO$^+$ ILC2 with features of activated cells prompted us to investigate whether resting CD45RA$^+$ ILC2s can convert into inflammatory CD45RO$^+$ cells. Purified PB CD45RA$^+$

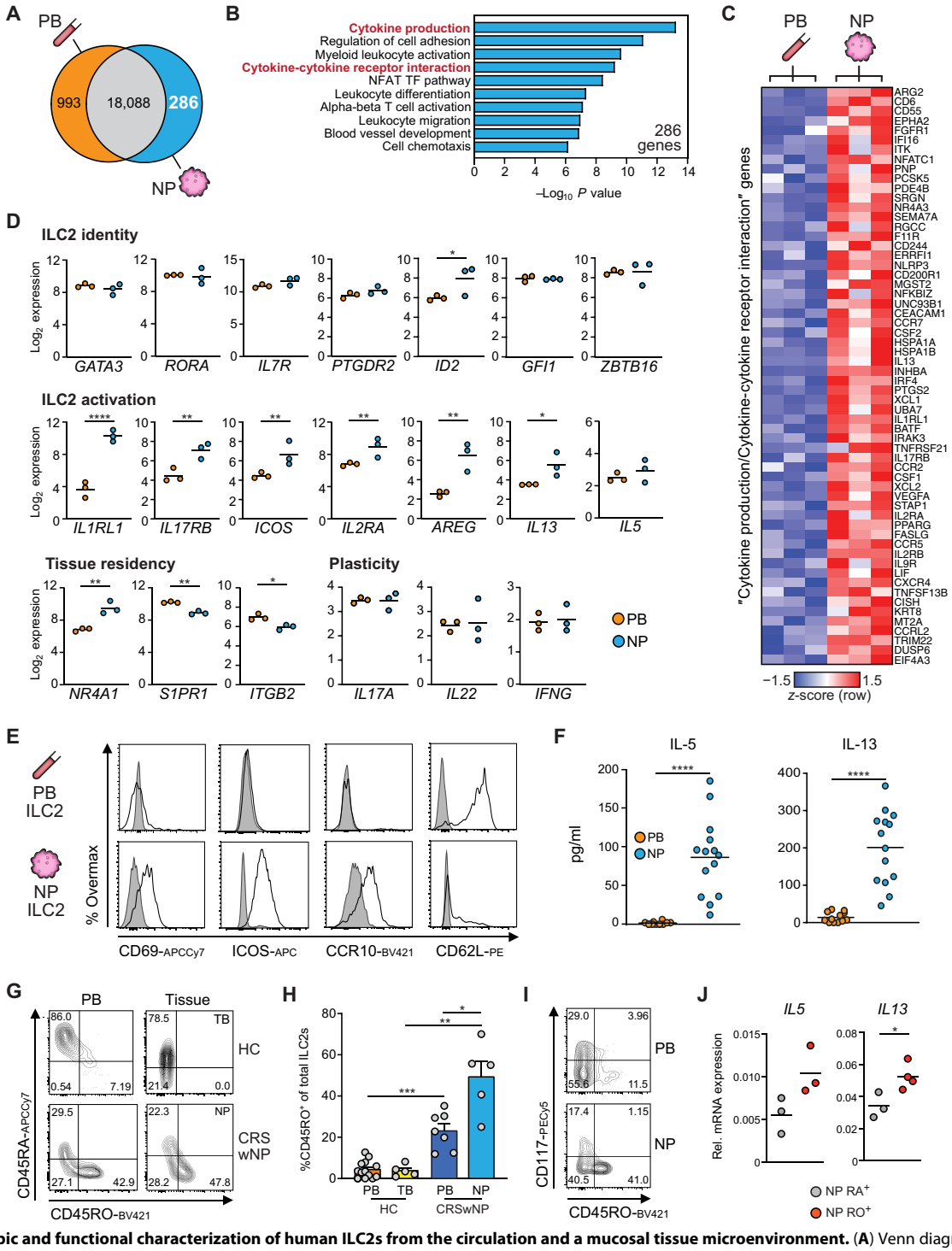

Fig. 1. Phenotypic and functional characterization of human ILC2s from the circulation and a mucosal tissue microenvironment. (**A**) Venn diagram showing the number of differentially expressed genes (adjusted $P < 0.05$) between PB and NP ILC2s. (**B**) Pathway enrichment analysis of the 286 genes up-regulated in NP ILC2s. (**C**) Heatmap of mRNA expression values for genes associated with the "Cytokine production" and the "Cytokine-cytokine receptor interaction" biological pathways highlighted in (B). (**D**) Log_2 mRNA expression values of selected genes involved in ILC2 identity, ILC2 activation, tissue residency, and plasticity. (**E**) Flow cytometric characterization of activation-associated surface markers and chemokine receptors on PB (top) and NP (bottom) ILC2s. Signals from isotype-matched control antibodies are indicated in dark gray. (**F**) IL-5 and IL-13 levels measured by ELISA in culture supernatant from PB and NP ILC2 grown for 7 days in medium with IL-2. (**G**) CD45RA and CD45RO surface expression on ILC2s isolated from PB and noninflamed nasal TB tissue samples of HC individuals or from PB and NP samples of patients with CRSwNP. (**H**) Quantification of $CD45RO^+$ ILC2s in the indicated PB and tissue samples from multiple individuals. (**I**) CD117 and CD45RO surface expression on PB and NP ILC2s. (**J**) Relative mRNA expression (to *GAPDH*) of *IL5* and *IL13* in $CD45RA^+$ and $CD45RO^+$ ILC2s isolated from NP tissue as measured by qPCR. Data from (E), (G), and (I) are representative of at least three donors from more than three independent experiments. Error bars in (H) indicate SEM. $^*P < 0.05$, $^{**}P < 0.01$, $^{***}P < 0.001$, and $^{****}P < 0.0001$ [Mann-Whitney *U* test and moderated *t* test corrected for multiple testing in (D)].

ILC2s cultured in the presence of only IL-2 and IL-7 barely expressed CD45RO or the known activation markers CD25 and ICOS (Fig. 2A). In contrast, various (combinations of) activating cytokines induced robust conversion into a CD45RO$^+$ICOS$^+$CD25$^+$ inflammatory phenotype resembling that of NP ILC2s (Fig. 2, A and B, and fig. S2A). IL-33 or IL-1β was required for this process because the three signal transducer and activator of transcription 5 (STAT5)–activating cytokines IL-2, IL-7, and TSLP together induced only limited CD45RA-to-CD45RO conversion (Fig. 2B), suggesting that STAT5 activation by itself is not sufficient for efficient induction of the CD45RO$^+$ phenotype. PB CD45RA$^+$ cells cultured with IL-33 alone showed poor survival and no CD45RA-to-CD45RO conversion, even at earlier time points (fig. S2, B and C).

Given the relevance of the alarmins IL-33 and TSLP for ILC2 activation in the lung and the elevated expression of TSLP in NP as compared with TB tissue (*45*), we primarily focused on this cytokine combination as a potent inducer of the CD45RA-to-CD45RO phenotypic switch. Upon activation of CD45RA$^+$ PB ILC2s with IL-2, IL-33, and TSLP, the induced CD45RO$^+$ cells showed an up-regulation of *IL5*, *IL13*, and *IL9* mRNA levels (fig. S2D). Phorbol 12-myristate 13-acetate (PMA) and ionomycin restimulated CD45RO$^+$ ILC2s had the highest capacity to produce IL-5 (and to a lesser extent IL-9; Fig. 2, C and D, and fig. S2E), whereas CD45RA$^+$ and CD45RO$^+$ cells showed a similar capacity to produce IL-13 (fig. S2E). These data indicate that resting CD45RA$^+$ ILC2s are primed to produce

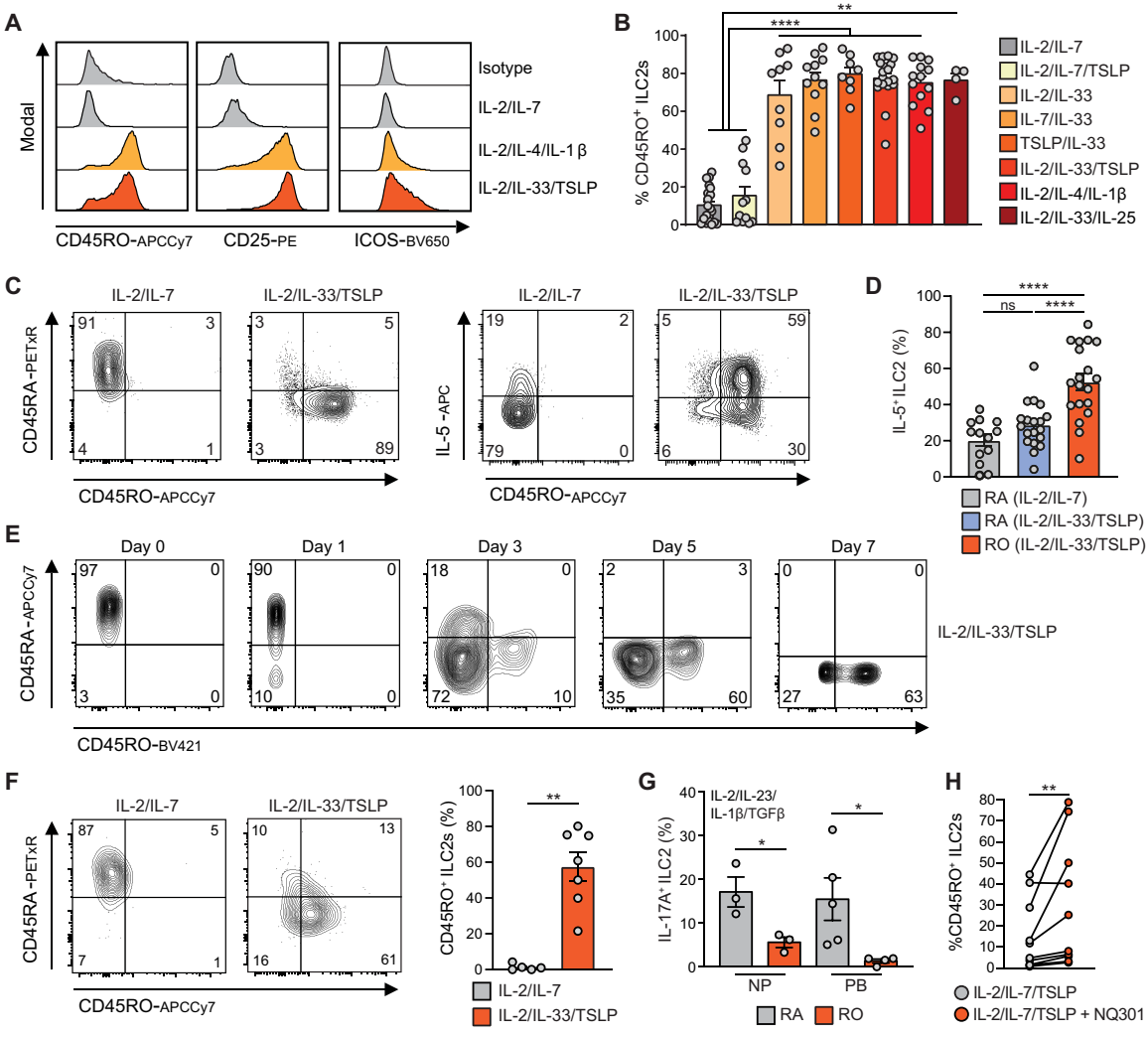

Fig. 2. In vitro differentiation of resting CD45RA$^+$ ILC2s into inflammatory CD45RO$^+$ ILC2s. (**A**) Flow cytometry measurement of CD45RO, CD25, and ICOS expression on CD45RA$^+$ PB ILC2s cultured in the presence of the indicated cytokines. (**B**) Quantification of CD45RO$^+$ ILC2s after 7 days of culturing sorted PB CD45RA$^+$ ILC2s with the indicated cytokines. (**C**) Flow cytometry quantification of CD45RA/CD45RO expression (left) and IL-5/CD45RO expression (right) after culture with the indicated cytokines. (**D**) Percentage of IL-5–expressing cells in CD45RA$^+$ or CD45RO$^+$ PB ILC2s after culturing of sorted PB CD45RA$^+$ ILC2s with the indicated cytokines. ns, not significant. (**E**) Flow cytometry time-course analysis of CD45RA/CD45RO expression during a 7-day culture of CD45RA$^+$ PB ILC2s with IL-2, IL-33, and TSLP. (**F**) CD45RA and CD45RO expression after at least 20 days of culture of single CD45RA$^+$ PB ILC2s on OP9-DL4 stromal cells with indicated stimuli. Bar graph shows a quantification of CD45RO expression on populations grown from single clones with the indicated cytokines. (**G**) Percentage of IL-17A–expressing cells in CD45RA$^+$ or CD45RO$^+$ ILC2s cultured with IL-2, IL-23, IL-1β, and TGFβ. ILC2s were sorted from NP or PB. (**H**) Proportions of CD45RO$^+$ ILC2s after culture of CD45RA$^+$ ILC2s in the presence of IL-2, IL-7, and TSLP with or without the CD45 phosphatase inhibitor NQ301. Data from (A) to (H) [exception, (F)] were obtained by starting with CD45RA$^+$ ILC2s isolated from PB of healthy donors and cultured for 7 days with indicated stimuli. Data from (A), (C), and (E) are representative of at least three donors from more than three independent experiments. Symbols represent individual donors; bars indicate mean values ± SEM. *$P < 0.05$, **$P < 0.01$, ***$P < 0.001$, and ****$P < 0.0001$ (Mann-Whitney *U* test).

IL-13 but not IL-5 (and IL-9), whereas CD45RO$^+$ ILC2s produce high levels of all three cytokines under these conditions. CD45RA$^+$ PB ILC2s exposed to IL-2/IL-33/TSLP for 7 days first down-regulated CD45RA, resulting in the formation of a CD45RA^{low} population, which was followed by up-regulation of CD45RO (Fig. 2E). Clones of CD45RA$^+$ ILC2s generated on OP9 stromal cells stably maintained their phenotype in the presence of survival signals (IL-2/IL-7) and converted to CD45RO$^+$ cells when exposed to activating cytokines (Fig. 2F).

ILC2s can exhibit substantial functional plasticity when exposed to polarizing cytokines such as IL-12 or IL-23 (*15*). To test the potential for plasticity in CD45RO$^+$ cells, we cultured PB CD45RA$^+$ and CD45RO$^+$ ILC2s (either freshly sorted or generated in vitro by culturing CD45RA$^+$ for 7 days with IL-2/IL-33/TSLP) in medium containing type 1 (IL-2/IL-12/IL-18), type 2 (IL-2/IL-33/TSLP), or type 3 [IL-2/IL-23/IL-1β/transforming growth factor β (TGFβ)] conditions. CD45RO$^+$ ILC2s produced less interferon γ (IFNγ) or IL-17 under plasticity-inducing conditions and maintained high IL-5 levels when exposed to strong inducers of type 1 or type 3 cytokine synthesis (fig. S2F). Similar results were obtained using sorted CD45RA$^+$ and CD45RO$^+$ ILC2s from NPs (Fig. 2G). These findings show that CD45RO$^+$ ILC2s display robust type 2 polarization and have less potential for plasticity than their CD45RA$^+$ counterparts.

In T cells, CD45 phosphatase activity appears to be restrained by homodimerization, which is facilitated by the smaller size of the CD45RO extracellular domain as compared with the larger CD45RA molecule (*42*). As CD45 isoforms are able to control the relative sensitivity threshold to external stimuli in various immune cells (*42*), we hypothesized that the enhanced phosphatase activity of CD45RA might impose a signaling threshold on resting CD45RA$^+$ ILC2s for activating cytokines. To test this, we isolated CD45RA$^+$ PB ILC2s and cultured them in the presence of IL-2, IL-7, and TSLP (a relatively weak stimulus; Fig. 2B), with or without the CD45 phosphatase inhibitor NQ301 (*46*). Conversion into a CD45RO$^+$ phenotype and IL-5 production were enhanced in the presence of NQ301 (Fig. 2H and fig. S2G), indicating that CD45 phosphatase inhibition sensitizes CD45RA$^+$ ILC2s to cytokine signaling.

Together, these data show that cytokine stimulation induces conversion of CD45RA$^+$ ILC2s into potent cytokine-producing CD45RO$^+$ cells, and that CD45RA phosphatase activity can restrain the activation of resting CD45RA$^+$ ILC2s.

Conversion of ILC2s into a CD45RO$^+$ inflammatory phenotype is tightly linked to BATF and IRF4 transcription factor activity

To compare CD45RO$^+$ ILC2s generated in vitro with NP ILC2s on a transcriptome-wide level, we generated microarray gene expression data from PB ILC2s after 7 days of stimulation with IL-2, IL-33, and TSLP. As expected, genes involved in cytokine-mediated signaling and ILC2 activation (e.g., *IL2RA*, *IL13*, *IL1RL1*, *IL17RB*, and *IL9R*) were up-regulated in both cytokine-stimulated PB and NP ILC2s as compared with freshly isolated resting PB ILC2s (Fig. 3A and fig. S3, A to C).

To better understand the molecular drivers of the CD45RO$^+$ inflammatory ILC2 phenotype, we combined our gene expression data with previously generated epigenome maps of PB ILC2s (*12*). Profiling H3K4Me2$^+$ active genes and regulatory elements across the genome of resting PB ILC2s and cytokine-stimulated (with IL-2/IL-25/IL-33) ILC2s identified ~3500 gene regulatory elements that increased more than fourfold in H3K4Me2$^+$ signal upon CD45RA-to-CD45RO conversion (Fig. 3B and fig. S3D). This epigenetic "signature" of the CD45RO$^+$ inflammatory ILC2 phenotype was enriched for genes involved in cytokine signaling and proliferation pathways (fig. S3E). Transcription factor binding motif enrichment analysis revealed six transcription factor families strongly associated with epigenome activation during CD45RA-to-CD45RO conversion (Fig. 3C), including motifs for factors important for lymphocyte biology such as GATA, ETS, AP-1, RUNX, IRF, and NF-κB (nuclear factor κB) family proteins. Hierarchical clustering of gene expression profiles for the 95 transcription factors belonging to these six families in resting PB, NP, and cytokine-stimulated PB ILC2s revealed distinct gene expression profiles (fig. S3F and table S2). Around half of the transcription factors (n = 46) showed invariant moderate-to-low expression levels, whereas several factors showed (weak) up-regulation (i.e., *GATA2*, *ETV5*, and *ATF3*) or strong down-regulation (e.g., *IRF1*, *FOS*, and *JUN*) specifically in activated PB or NP ILC2s (Fig. 3D and fig. S3F). Other factors, including proteins implicated in ILC biology such as GATA3, ETS1, and RUNX1 (*47*), were expressed at high levels not only in CD45RO$^+$ ILC2s but also in CD45RA$^+$ cells and were therefore unlikely to drive CD45RA-to-CD45RO conversion (Fig. 3D and fig. S3F). Out of 95 transcription factor genes, only 3 showed expression patterns that correlated with the CD45RO$^+$ cell abundance in our ILC2 samples (i.e., lowest in resting PB ILC2s, increased in NP ILC2s, and highest in cytokine-stimulated PB ILC2s). The CREM (AP-1 family) but especially BATF (AP-1 family) and IRF4 transcription factors were strongly associated with CD45RO$^+$ ILC2 abundance (Fig. 3D). The strong induction of *BATF* and *IRF4* in ILC2s after alarmin exposure was confirmed by a substantial increase in H3K4Me2 levels at their genomic loci (fig. S3G). Our data implicate BATF and IRF4 as critical regulators of CD45RA-to-CD45RO ILC2 conversion, in line with the prominent roles these factors play in immune cell activation (*48*–*50*).

To substantiate this hypothesis, we measured BATF, IRF4, and CD45RO protein expression dynamics after CD45RA$^+$ ILC2 activation. Using different cytokine combinations, we noticed a marked correlation between the proportions of CD45RO$^+$ and IRF4$^+$ or BATF$^+$ ILC2s after 7 days of culture ($R \geq 0.9$ and $P \leq 0.0001$; fig. S3H). IRF4 and BATF activation preceded CD45RO expression at early time points (Fig. 3, E and F). The vast majority (>90%) of CD45RO$^+$ ILC2s generated during the time course were IRF4 and BATF double-positive (Fig. 3G). A critical cooperative role of BATF and IRF4 in promoting CD45RA-to-CD45RO ILC2 conversion was further supported by a significant enrichment of BATF-IRF composite binding motifs within H3K4Me2$^+$ regulatory elements unique to CD45RO$^+$ ILC2s (fig. S3I). Last, T-5224, a selective small-molecule inhibitor of AP-1 family transcription factor binding (*51*), significantly limited CD45RA-to-CD45RO conversion induced by IL-2, IL-33, and TSLP (Fig. 3H).

In T cells, the CD45RA-to-CD45RO splicing isoform switch is controlled by the induction of the hnRNPLL RNA binding protein (*52*). In ILC2s, *hnRNPLL* expression was positively correlated to CD45RO$^+$ ILC2 frequencies (similar to BATF and IRF4; fig. S3J). RNA sequencing revealed no detectable *hnRNPLL* transcripts in freshly isolated PB CD45RA$^+$ ILC2s, whereas in vitro CD45RA-to-CD45RO conversion with IL-2, IL-33, and TSLP induced robust *hnRNPLL* expression (fig. S3J). Additional H3K4Me2 signals appeared around

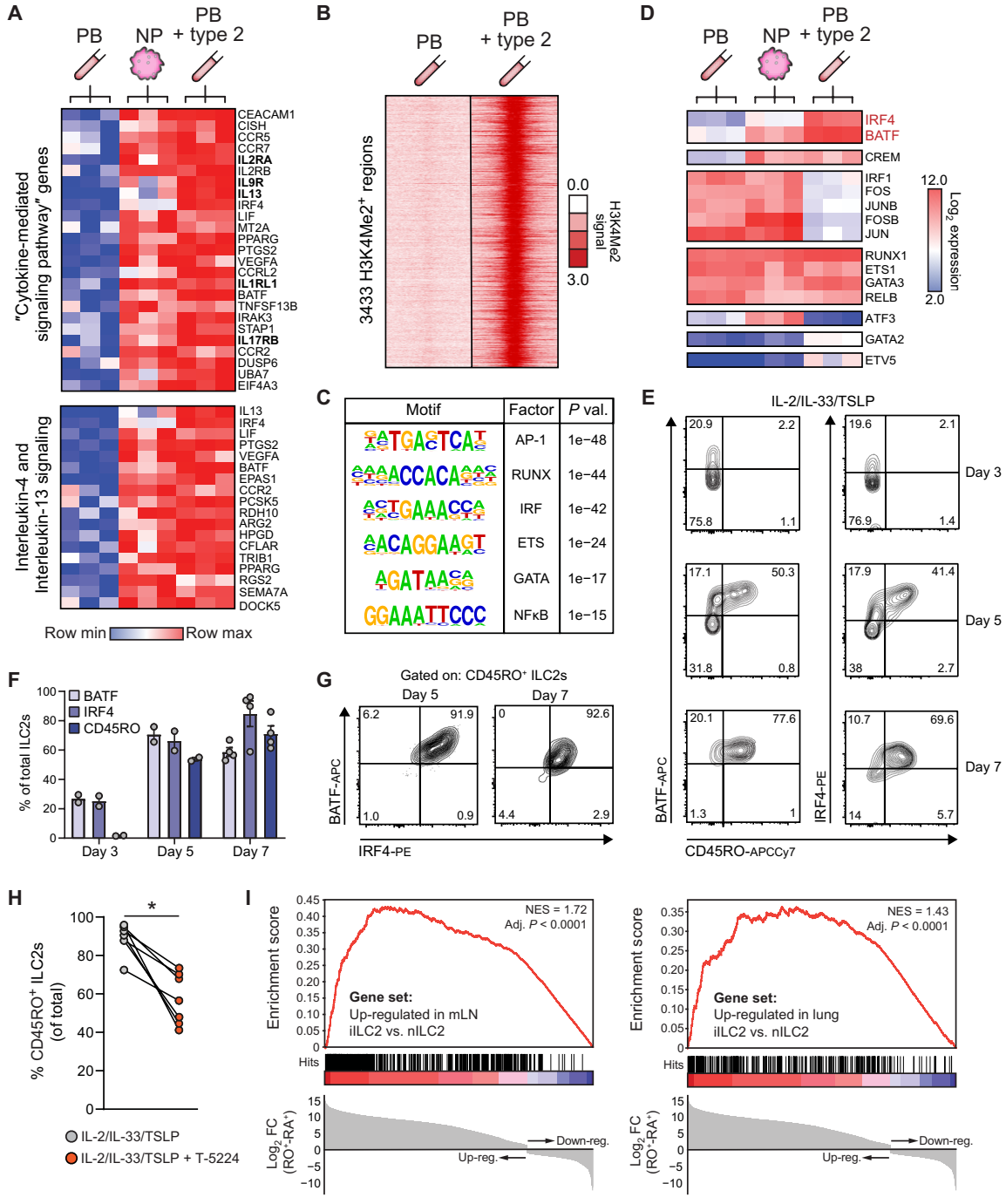

Fig. 3. ILC2 conversion into a CD45RO$^+$ inflammatory phenotype akin to mouse iILC2s is associated with BATF and IRF4 transcription factor activity. (**A**) Heatmap showing mRNA expression levels of genes associated with "Cytokine-mediated signaling pathways" (top) and "IL-4 and IL-13 signaling" (bottom) for PB ILC2s, NP ILC2s, and PB ILC2s cultured for 7 days in the presence of IL-2, IL-33, and TSLP ("PB + type 2"). (**B**) Heatmap depicting normalized H3K4Me2 ChIP-sequencing signal intensity at 3433 regulatory regions that showed substantial activation (more than fourfold signal increase) in PB + type 2 ILC2s as compared with resting PB ILC2s. (**C**) Transcription factor motif enrichment within the 3433 H3K4Me2$^+$ regulatory regions shown in (B). The six most significantly overrepresented binding motifs (based on *P* value) are shown. (**D**) Heatmap showing mRNA expression levels of selected genes belonging to the six transcription factor families identified in (C) (see fig. S3F for all genes). (**E** and **F**) Flow cytometry time-course analysis of CD45RO, BATF, and IRF4 protein expression during a 7-day culture of CD45RA$^+$ PB ILC2s with IL-2, IL-33, and TSLP. Quantifications are shown in (F). (**G**) Representative flow cytometry analysis of BATF and IRF4 expression in CD45RO$^+$ ILC2s after 5 or 7 days of culture with IL-2/IL-33/TSLP. (**H**) Proportions of CD45RO$^+$ ILC2s after culture of CD45RA$^+$ ILC2s in the presence of IL-2, IL-33, and TSLP with or without the AP-1 family inhibitor T-5224. (**I**) GSEA using differentially expressed genes between PB (CD45RA$^+$) and PB + type 2 (CD45RO$^+$) ILC2s (from RNA sequencing of $n = 3$ pairs; adjusted $P < 0.1$) preranked on the basis of their $\log_2$ fold change (CD45RO$^+$-CD45RA$^+$; indicated below in gray). Enrichment was calculated for two sets of genes that were previously found up-regulated in mouse iILC2 as compared with nILC2 from mesenteric lymph nodes (mLN) (*21*) or lung tissue (*18*). Adjusted (Adj.; false discovery rate method) *P* values are shown. *$P < 0.05$ (Wilcoxon matched-pairs signed-rank test). TF, transcription factor; NES, normalized enrichment score

the *hnRNPLL* gene promoter during CD45RA-to-CD45RO ILC2 conversion, in line with increased transcriptional activation of the locus and similar to differences seen between CD45RA$^+$ and CD45RO$^+$ CD4$^+$ T cells (fig. S3K). More specifically, the intronic accumulation of H3K4Me2 signal in CD45RO$^+$ ILC2s and CD4$^+$ T cells coincided with the occurrence of two BATF/IRF composite motifs, which are bound by BATF in mouse T_H17 cells (fig. S3K) (*53*). Together, our analyses indicate that induction of a CD45RO$^+$ inflammatory phenotype in human ILC2s requires BATF/IRF4 transcription factor activity and supports a model in which cooperative BATF/IRF4 binding activates hnRNPLL expression, which results in alternative splicing of CD45 mRNA and production of the CD45RO isoform.

Human CD45RO$^+$ ILC2s are transcriptionally akin to migratory mouse iILC2s

The formation of mouse iILC2s was recently shown to rely on BATF (*20*). To assess in a more unbiased fashion how the human CD45RO$^+$ ILC2 phenotype is related to the mouse nILC2/iILC2 subsets, we performed gene set enrichment analysis (GSEA) using published transcriptional signatures of nILC2s and iILC2s isolated from the lung (*18*) or mesenteric lymph node (*21*). Genes differentially expressed between CD45RA$^+$ PB ILC2s and cytokine-induced CD45RO$^+$ ILC2s were ranked according to their fold change and used as input for GSEA. We observed strong positive enrichments (adjusted $P < 0.0001$) for genes up-regulated in CD45RO$^+$ ILC2s using both iILC2 signature gene sets (Fig. 3I), whereas no significant enrichments were detected with nILC2 signature gene sets (adjusted $P > 0.05$). About 30% of the genes that define iILC2s in vivo (i.e., expressed significantly higher in iILC2s versus nILC2s) are also up-regulated during the CD45RA-to-CD45RO ILC2 conversion ($P < 0.0001$, Fisher's exact test; fig. S3L). These data show that human CD45RO$^+$ ILC2s are transcriptionally akin to mouse iILC2s, strongly suggesting that these ILC2 subsets are functionally equivalent.

Elevated levels of circulating CD45RO$^+$ ILC2s in uncontrolled steroid-resistant asthma

Our observation that patients with CRSwNP showed substantial levels of CD45RO$^+$ ILC2s not only in inflamed NP tissue but also in their circulation (Fig. 1, G and H) prompted us to further evaluate ILC2 CD45 status as a blood biomarker for type 2 inflammatory disease. Given the potential pathogenic role of ILC2s in asthma (*28*), we investigated the PB ILC2 phenotype in a cohort of 61 clinically well-characterized asthma patients and 17 HCs. These patients were selected to represent individuals with different levels of symptom control and exacerbation frequencies (table S3). From 22 patients with asthma, we also obtained PB samples during an active exacerbation. Whereas the frequencies of ILC2s did not differ between PB samples from HCs and asthma patients (fig. S4A), we did observe a clear trend toward increasing proportions of CD45RO$^+$ cells within the ILC2 population in PB samples from all asthma patients ($P = 0.086$; Fig. 4A). When patients were grouped according to their level of symptom control [based on Asthma Control Questionnaire (ACQ) scores (*54*): controlled, 0 to 0.75; partially controlled, 0.75 to 1.5; uncontrolled, >1.5], we observed a significant increase in PB CD45RO$^+$ ILC2 levels specifically in the subset of patients suffering from uncontrolled disease (Fig. 4B). In agreement with this, ACQ scores and CD45RO$^+$ ILC2 proportions were positively correlated across our patient cohort (fig. S4B). When patients with asthma were subdivided on the basis of exacerbation frequencies, we again observed increased proportions of PB CD45RO$^+$ ILC2 in patients with frequent exacerbations (>2 during the previous winter season) (Fig. 4C). In addition, comparison of paired PB samples obtained from asthma patients at baseline (stable disease) and during an exacerbation revealed an increase in circulating CD45RO$^+$ ILC2s during exacerbations for 71% of patients (>1.25-fold change; Fig. 4, D and E).

Because uncontrolled asthma with frequent exacerbations is associated with poor response to inhaled corticosteroid treatment, we investigated the relationship between steroid dose, symptom control, and CD45RO$^+$ ILC2 levels. Asthma patients on a high inhaled steroid dose (>1000 equivalent units; see Materials and Methods for dose definitions) had significantly more PB CD45RO$^+$ ILC2s compared with patients with a relatively low inhaled steroid intake (fig. S4C). Similarly, asthma patients with above-average CD45RO$^+$ ILC2 proportions (as measured across the entire cohort; shown in Fig. 4A) required overall higher steroid doses than patients with lower than average CD45RO$^+$ ILC2 proportions (Fig. 4F). Last, we observed significantly elevated frequencies of PB CD45RO$^+$ ILC2s in patients with uncontrolled steroid-resistant asthma (ACQ > 1.5 despite a >1000-steroid equivalent unit dose) as compared with steroid-sensitive patients (ACQ < 0.75 with any steroid dose) (Fig. 4G). Receiver operating characteristic (ROC) curve analysis revealed a statistically significant predictive value of PB CD45RO$^+$ ILC2 levels to separate steroid-sensitive from steroid-resistant patients with asthma (fig. S4D). Overall, these data show that the presence of circulating inflammatory CD45RO$^+$ ILC2s is linked to severe asthma, asthma exacerbations, and steroid resistance.

The CD45RO$^+$ inflammatory phenotype confers steroid resistance to ILC2s

To further explore the potential link between the CD45 isoform status on ILC2s and steroid resistance, we investigated the sensitivity of both CD45RA$^+$ and CD45RO$^+$ ILC2s to dexamethasone, a potent immunosuppressive corticosteroid. To facilitate comparison of CD45RA$^+$ and CD45RO$^+$ ILC2s, we generated the latter by first stimulating sorted CD45RA$^+$ ILC2s with IL-2 and IL-33 or with IL-2, IL-33, and TSLP for 7 days in vitro before dexamethasone treatment. Exposing CD45RA$^+$ ILC2s to a nontoxic dose (fig. S5A) of dexamethasone for 7 days resulted in strong inhibition of cytokine-driven CD45RO induction, whereas minimal effects were observed on the phenotype of CD45RO$^+$ cells (Fig. 5, A and B, and fig. S5B). Similar results were obtained using IL-7/IL-33 or TSLP/IL-33 cytokine combinations (fig. S5C). In addition, cytokine-induced proliferation of CD45RA$^+$ ILC2s upon cytokine exposure was greatly reduced by dexamethasone, whereas CD45RO$^+$ ILC2 proliferation was unaffected or even slightly enhanced (Fig. 5, C and D). On average, production of IL-5 and IL-13 by CD45RA$^+$ ILC2s in response to IL-33 was reduced by 92% and 65%, respectively, when treated with dexamethasone, compared with a ~10 to 30% reduction for CD45RO$^+$ ILC2s (Fig. 5, E to G). Similar levels of steroid-resistant cytokine production were evoked when CD45RA-to-CD45RO conversion was induced using IL-2 and IL-33 or IL-2, IL-33, and TSLP (fig. S5D), indicating that steroid resistance in CD45RO$^+$ ILC2s is promoted by STAT5-activating cytokines but does not strictly require TSLP. In agreement with the robust steroid resistance of CD45RO$^+$ ILC2s generated in vitro, NP ILC2s (strongly enriched for tissue CD45RO$^+$ ILC2s; see Fig. 1H) showed significantly less sensitivity to dexamethasone as measured by intracellular IL-5 staining and secreted IL-5 levels in culture supernatant

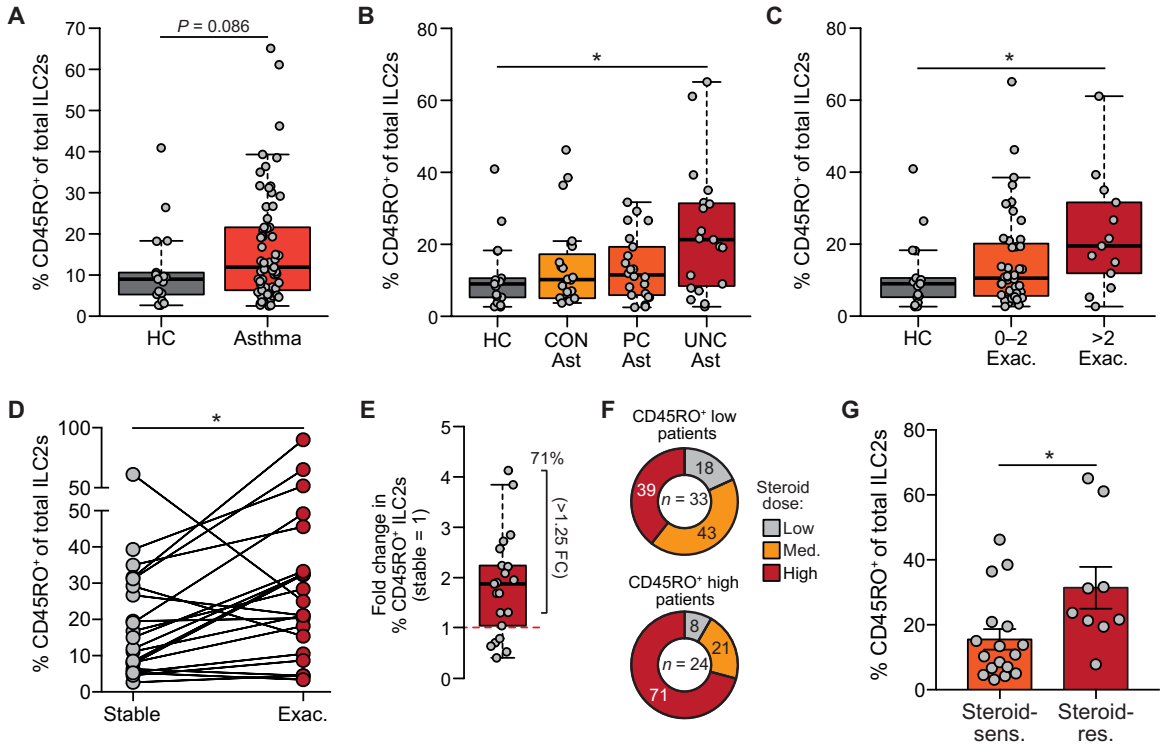

Fig. 4. Circulating CD45RO$^+$ ILC2 frequencies are increased in uncontrolled and steroid-resistant asthma. (**A**) Quantification of CD45RO$^+$ ILC2s using flow cytometry in PB samples of 17 HC individuals and 61 patients with asthma. (**B**) Quantification of CD45RO$^+$ ILC2s in PB samples of HC individuals, controlled asthma (CON Ast; ACQ < 0.75), partially controlled asthma (PC Ast; ACQ = 0.75 to 1.5), and uncontrolled asthma (UNC Ast; ACQ > 1.5) patients. (**C**) Quantification of CD45RO$^+$ ILC2s in PB samples of HC individuals and patients with asthma with zero to two exacerbations ("Exac.") or more than two exacerbations in the previous year. (**D**) Quantification of CD45RO$^+$ ILC2s in 22 paired PB samples of patients with asthma during stable disease and during an active exacerbation. (**E**) Fold change (FC) in the percentage of CD45RO$^+$ ILC2s in PB samples of patients with asthma during an active exacerbation, in which the percentage of CD45RO$^+$ ILC2s during stable disease was set to 1. Seventy-one percent of patients showed an FC of >1.25. (**F**) Pie charts summarizing proportions of patients with asthma with low (0 to 500 dose equivalent units, see Materials and Methods for details), medium (500 to 1000 dose equivalent units), and high (>1000 dose equivalent units) inhaled corticosteroid intake for two groups of patients: those with lower than average [16.78%, based on all 61 patients shown in (A)] CD45RO$^+$ ILC2 frequencies ("CD45RO$^+$ low") and those with higher than average CD45RO$^+$ ILC2 frequencies ("CD45RO$^+$ high"). (**G**) Quantification of CD45RO$^+$ ILC2s in PB samples of patients with asthma characterized as steroid sensitive (sens.; ACQ < 0.75, on any steroid dose) and steroid resistant (res.; ACQ > 1.5, on >1000 dose equivalent units). Symbols represent individual donors; bars indicate mean values ± SEM. *P < 0.05 (Mann-Whitney U test or Kruskal-Wallis test corrected for multiple testing).

(Fig. 5, H and I). In summary, these experiments reveal that IL-2 and IL-33 are sufficient to induce inflammatory CD45RO$^+$ ILC2s that are resistant to suppression by corticosteroids, the mainstay of therapy for chronic type 2 inflammatory disorders.

Corticosteroids suppress CD45RA-to-CD45RO conversion and induce a distinct ILC2 phenotype

Gene expression analysis (using RNA sequencing) of CD45RA$^+$ ILC2s activated with IL-2, IL-33, and TSLP in vitro for 7 days in the presence or absence of dexamethasone revealed a steroid-sensitive gene expression program consisting of 452 genes (Fig. 6A). Genes suppressed by dexamethasone (n = 266), e.g., *IL5*, *IL13*, and *CSF2*, associated with an interconnected network of biological pathways critical for inflammatory type 2 effector cells (Fig. 6, B and C, and fig. S6A). In contrast, dexamethasone also activated a subset of 186 genes, which showed only a minor overlap (8.6%) with genes expressed at higher levels in CD45RA$^+$ ILC2s as compared with CD45RO$^+$ ILC2s (n = 16; adjusted P < 0.05). Genes up-regulated by dexamethasone included *DUSP1*, a canonical target gene of glucocorticoid receptor (GR) signaling that encodes the DUSP1/MKP1 phosphatase, an inhibitor of the mitogen-activated protein kinase (MAPK) signaling pathway that operates downstream of the IL-33 receptor (Fig. 6D) (*55*, *56*). Up-regulated genes also encode proteins involved in tissue repair and remodeling (e.g., *AREG* and *PDGFA*), enhanced migratory capacity (*KLF2*, *S1PR1*, and *CXCR4*), and immune modulation (*HAVCR2* encoding TIM-3, *CD86*, and *CD9*) (Fig. 6D and fig. S6, B and C). In addition, whereas canonical ILC2 regulator genes *GATA3* and *PTGDR2* (encoding CRTH2) were unaffected, dexamethasone up-regulated the transcription factors *ETV5* and *CBFB* (fig. S6B). In mouse models of allergic airway inflammation, Etv5 has been implicated in shaping T_H cell differentiation (*57*, *58*), whereas Cbfb was shown to restrain steady-state ILC2 activation and prevent exhaustion upon activation (*59*). Thus, dexamethasone induces differentiation of CD45RA$^+$ ILC2s toward a phenotypically distinct, less inflammatory, and more immunomodulatory cell population.

Unique metabolic reprogramming of CD45RO$^+$ ILC2s is linked to steroid resistance

Unlike their CD45RA$^+$ counterparts, CD45RO$^+$ ILC2s maintain high levels of type 2 cytokine production and proliferation in the presence of corticosteroids. This phenotypic distinction could not be

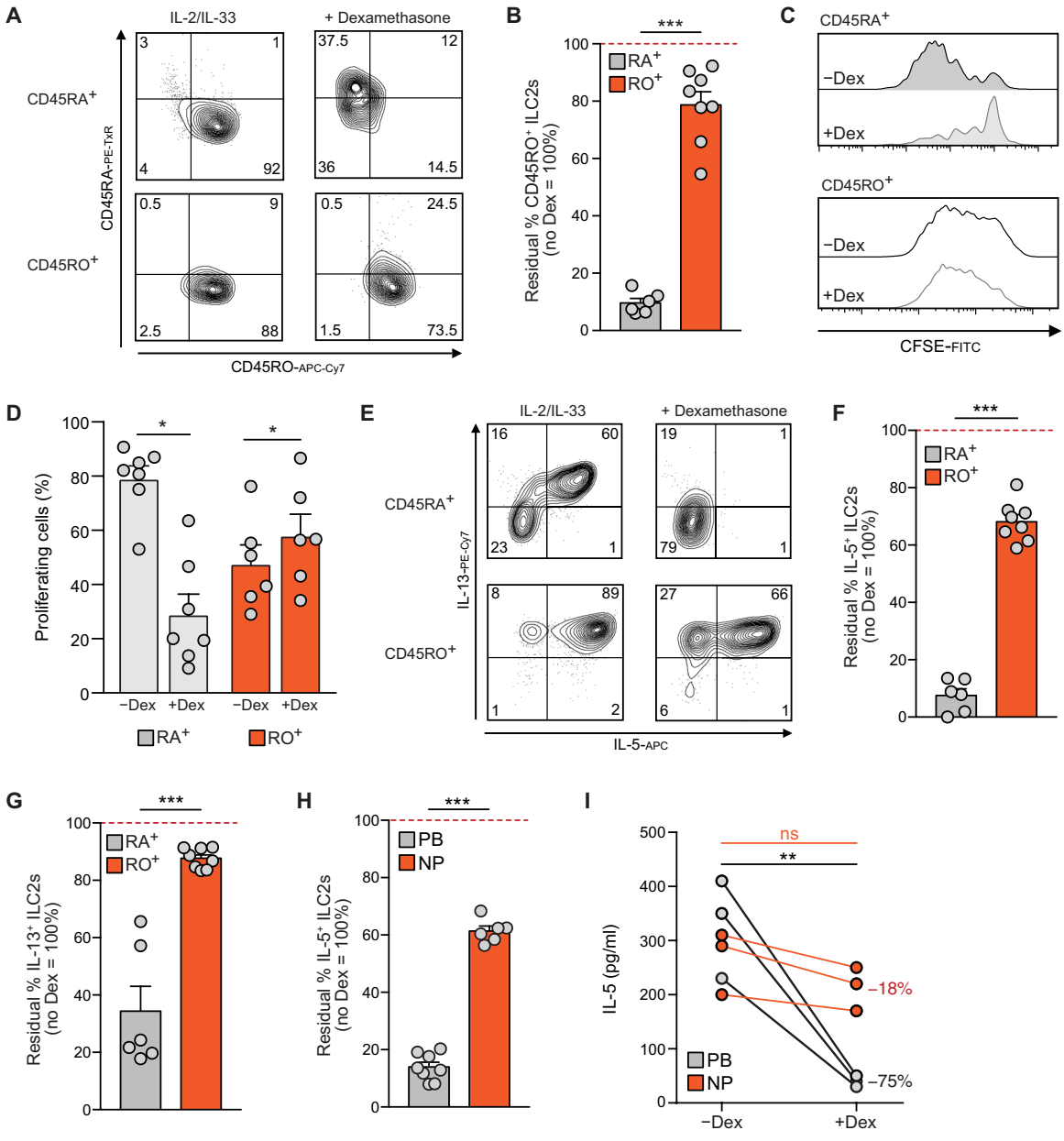

Fig. 5. CD45RO$^+$ inflammatory ILC2s are resistant to suppression by corticosteroids. (**A**) Flow cytometry analysis of CD45RA and CD45RO expression on ILC2s cultured in the presence of IL-2/IL-33 with or without dexamethasone for 7 days. Top panels show results when starting with sorted CD45RA$^+$ ILC2s. Bottom panels show effects on a CD45RO$^+$ ILC2 starting population, which was generated by culturing CD45RA$^+$ ILC2s with IL-2/IL-33 for 7 days before dexamethasone treatment. (**B**) Residual percentage of CD45RO$^+$ ILC2s after 7 days of culture in the presence of IL-2/IL-33 with dexamethasone as compared with without dexamethasone (Dex) when starting with CD45RA$^+$ (gray bars) or CD45RO$^+$ (red bars) ILC2s. (**C**) CFSE signal dilution by proliferation was measured by flow cytometry for labeled CD45RA$^+$ (top) and CD45RO$^+$ (bottom) ILC2s cultured for 4 days in the presence of IL-2/IL-33/TSLP with or without dexamethasone. (**D**) Frequencies of proliferating CD45RA$^+$ and CD45RO$^+$ ILC2s in the presence or absence of dexamethasone. (**E**) Flow cytometry analysis of intracellular IL-13 and IL-5 in indicated ILC2 populations cultured in the presence of IL-2/IL-33 with or without dexamethasone. (**F**) Residual percentage of IL-5$^+$ ILC2s after 7 days of culture in the presence of IL-2/IL-33 with dexamethasone as compared with without dexamethasone when starting with CD45RA$^+$ (gray bars) or CD45RO$^+$ (red bars) ILC2s. (**G**) Residual percentage of IL-13$^+$ ILC2s after 7 days of culture in the presence of IL-2 and IL-33 with dexamethasone as compared with without dexamethasone when starting with CD45RA$^+$ (gray bars) or CD45RO$^+$ (red bars) ILC2s. (**H**) Residual percentage of IL-5$^+$ ILC2s after 7 days of culture in the presence of IL-2/IL-33 with dexamethasone as compared with without dexamethasone when starting with sorted PB (gray bars) or NP (red bars) ILC2s. (**I**) IL-5 levels measured by ELISA in culture supernatant from sorted PB and NP ILC2s cultured for 7 days in the presence of IL-2/IL-4/IL-1β with or without dexamethasone. Data from (A), (C), and (E) are representative of at least three donors from more than three independent experiments. Symbols represent individual donors; bars indicate mean values ± SEM. *$P < 0.05$, **$P < 0.01$, and ***$P < 0.001$ (Mann-Whitney *U* test or paired Wilcoxon matched-pairs signed-rank test).

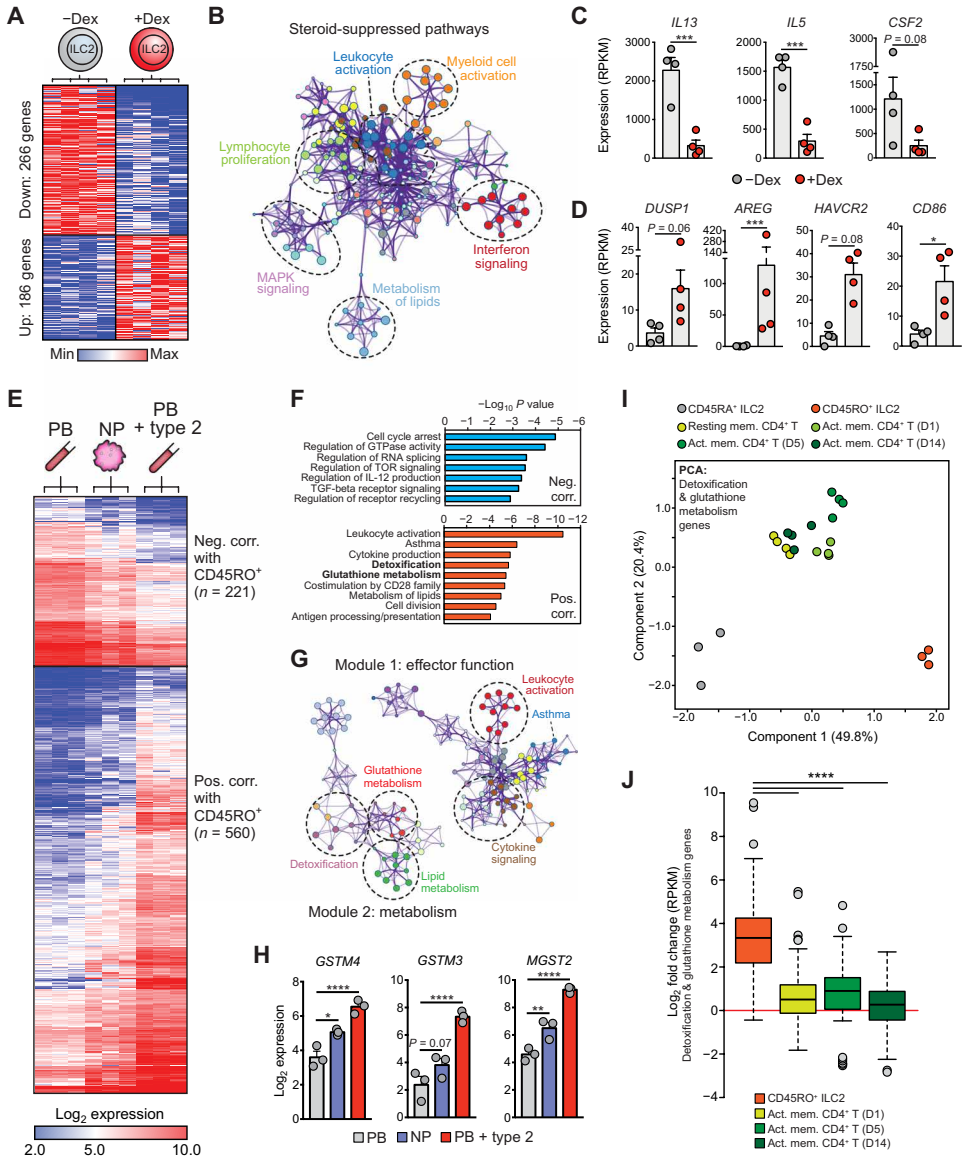

Fig. 6. Transcriptome analysis reveals phenotypic conversion of CD45RA$^+$ ILC2 by dexamethasone and metabolic reprogramming linked to steroid resistance. (**A**) Heatmap showing mRNA expression levels (RNA sequencing) of differentially expressed genes between CD45RA$^+$ ILC2s cultured for 7 days with IL-2/IL-33/TSLP in the presence or absence of dexamethasone. (**B**) Network of biological pathways suppressed in ILC2s activated by cytokines in the presence of dexamethasone. Spheres represent individual pathways that are connected and clustered (color-coded) on the basis of gene similarity. Nodes containing pathways associated with leukocyte activation, myeloid cell activation, lymphocyte proliferation, MAPK signaling, lipid metabolism, and interferon signaling are highlighted. Size of spheres indicates statistical significance ($P < 0.05$). (**C**) Expression levels (RPKM) of the pro-inflammatory genes *IL13*, *IL5*, and *CSF2* in ILC2s activated with or without dexamethasone. (**D**) Expression levels (RPKM) of canonical GR target *DUSP1* and the immunomodulatory genes *AREG*, *HAVCR2*, and *CD86* in ILC2s activated in the presence or absence of dexamethasone. (**E**) Heatmap showing mRNA expression levels of genes negatively (upper boxed part) or positively (lower boxed part) correlated with the increasing CD45RO$^+$ ILC2 frequencies found in PB ILC2s, NP ILC2s, or PB ILC2s cultured for 7 days in the presence of IL-2, IL-33, and TSLP (PB + type 2). Genes were ordered by gene expression pattern using *k*-means clustering ($k = 8$). (**F**) Pathway enrichment analysis of the 221 genes negatively correlated with CD45RO$^+$ ILC2 frequencies (top) and the 560 genes positively correlated with CD45RO$^+$ ILC2 frequencies (bottom). (**G**) Networks of biological pathways positively correlated with CD45RO$^+$ ILC2 frequencies, consisting of one module involved in effector function and one module involved in metabolism. Spheres represent individual pathways that are connected and clustered (color-coded) on the basis of gene similarity. Nodes containing pathways associated with asthma, cytokine signaling, leukocyte activation (module 1) or detoxification, lipid metabolism, and glutathione metabolism (module 2) are highlighted. Size of spheres indicates statistical significance ($P < 0.05$). (**H**) Expression levels ($\log_2$) of selected genes critical for glutathione metabolism in PB, NP, and PB + type 2 ILC2s. (**I**) Principal components analysis (PCA) of gene expression values ($\log_2$ RPKM) for the 78 genes within the detoxification and glutathione metabolism pathways that were positively correlated with CD45RO$^+$ ILC2 frequencies. CD4$^+$ T cell RNA-sequencing data were taken from a previously published time-course analysis of anti-CD3/CD28 stimulation of CD4$^+$CD45RO$^+$ T cells for the indicated days (D0, D1, D5, and D14) (*63*). (**J**) Boxplot showing combined $\log_2$ fold changes in expression (RPKM) of the genes used in (I). Fold changes were calculated by subtracting $\log_2$ expression values of activated cells (i.e., CD45RO$^+$ ILC2s and indicated T cells) from resting cells (i.e., CD45RA$^+$ ILC2s or resting memory CD4$^+$ T cells). Outliers are shown as individual dots. Symbols represent individual donors; bars indicate mean values ± SEM. *$P < 0.05$, **$P < 0.01$, ***$P < 0.001$, and ****$P < 0.0001$ (Wald test or Kruskal-Wallis test, both corrected for multiple testing). mem., memory; Act., activated.

explained by altered GR expression levels, as we did not detect marked changes in *NR3C1* (encoding the GR) mRNA levels between resting CD45RA$^+$ PB ILC2 and ILC2 populations strongly enriched for CD45RO$^+$ cells (i.e., NP ILC2s and PB ILC2s activated by cytokines in vitro) (fig. S6D).

To uncover the mechanistic basis of resistance to steroids in CD45RO$^+$ ILC2s in a more unbiased fashion, we mined our transcriptome data for genes with expression levels that were highly correlated to CD45RO$^+$ cell abundance (see above; lowest in resting PB ILC2s, increased in NP ILC2s, and highest in PB ILC2s that received type 2 cytokine stimulation). Using this approach, we identified 221 genes negatively correlating with CD45RO$^+$ cell abundance, which is associated with cell cycle arrest, mammalian target of rapamycin (mTOR) signaling, and receptor recycling. In contrast, 560 genes were positively correlated to CD45RO$^+$ ILC2 frequencies (Fig. 6, E and F). As expected, these included genes associated with ILC2 activation (e.g., *IL13* and *IL17RB*) and a network of pathways critical for effector function (Fig. 6, F and G). CD45RA-to-CD45RO conversion was coupled to extensive transcriptional changes of several metabolic pathways (Fig. 6, F and G). Although enhanced lipid metabolism is a

known hallmark of lymphocyte effector function (*60*), we also observed activation of metabolic pathways involved in intracellular detoxification and glutathione metabolism (Fig. 6, F and G). Glutathione *S*-transferases (GSTs) are detoxification enzymes that catalyze the conjugation of glutathione to a wide range of endogenous and exogenous compounds, including corticosteroids, ultimately leading to their elimination (*61*). Expression of genes encoding the glutathione synthetase, various GSTs (e.g., GSTM2 and MGST2), and other associated genes was positively correlated to CD45RO$^+$ ILC2 abundance (Fig. 6H and fig. S6E), providing a rationale for how the CD45RO$^+$ inflammatory ILC2 phenotype confers resistance to corticosteroids.

Unlike CD45RO$^+$ ILC2s, most CD4$^+$ T_H cells, including T_H2 cells, are sensitive to suppression by corticosteroids (*30*, *33*, *34*, *62*). Hence, we reasoned that the up-regulation of detoxification-associated genes observed in steroid-resistant CD45RO$^+$ ILC2s would be absent during CD4$^+$ T cell activation. To address this, we compared the induction of detoxification-associated genes after CD45RA-to-CD45RO ILC2 conversion and during a time-course activation of resting CD45RO$^+$ memory CD4$^+$ cells in vitro using anti-CD3/CD28 antibodies (*63*). Principal components analysis showed that steroid-resistant CD45RO$^+$ ILC2s formed a discrete cluster apart from steroid-sensitive CD45RA$^+$ ILC2s and memory CD4$^+$ T cells (Fig. 6I). Resting and activated memory CD4$^+$ T cells clustered closely together, indicating that metabolic reprogramming of detoxification pathways during cytokine-induced ILC2 activation is unique to ILC2s (Fig. 6I). This notion was further confirmed by the strongly reduced transcriptional induction of detoxification pathways associated with steroid resistance during memory CD4$^+$ T cell activation as compared with ILC2 CD45RA-to-CD45RO conversion (Fig. 6J). Similar differences were observed when comparing ILC2 and CD45RA$^+$ naive CD4$^+$ T cell activation (fig. S6F).

DISCUSSION

In this study, we identify an inflammatory ILC2 population marked by CD45RO that resides in inflamed mucosal tissue and can be detected in the circulation. This human ILC2 subset is transcriptionally akin to mouse iILC2s. Resting ILC2s, which express CD45RA, can convert into CD45RO$^+$ ILC2s upon cytokine exposure, which is tightly linked to activation of the BATF/IRF4 axis. CD45RO$^+$ inflammatory ILC2s are resistant to corticosteroids and increased in the circulation of patients with type 2 immunopathologies, correlating with a poor response to corticosteroid therapy and severe disease.

The CD45 isoform switch we observe upon activation of resting ILC2s is reminiscent of the well-known CD45RA-to-CD45RO switch that accompanies the activation of T cells. In mature naive T cells, CD45RA is gradually replaced by CD45RO on the cell surface upon T cell receptor stimulation (*42*). As observed in T cells, ILC2 CD45RA-to-CD45RO conversion is accompanied by activation of the hnRNPLL splicing regulator. The shorter extracellular domain of the CD45RO splicing isoform allows for homodimerization with reduced enzymatic activity, thereby altering the ability of the CD45 phosphatase to set a threshold for T cell receptor signals (*42*, *52*). Our data suggest that CD45 phosphatase inhibition can sensitize CD45RA$^+$ ILC2s to cytokine signaling, although the target(s) of CD45 in ILC2s remains unknown. Possible candidates expressed in ILC2s include Janus kinase (JAK) proteins (*64*) or the Src family kinase LCK (*65*). Dephosphorylation of signal transduction molecules by CD45RA might set a higher threshold for ILC2 activation, which would be relieved upon isoform switching to CD45RO.

In T cells, most of the previously activated naive cells stably maintain CD45RO expression, even after returning to a resting state as memory cells (*42*). Whether CD45RA-to-CD45RO switching is reversible in ILC2s or associated with "memory" ILC2s (*66*) remains to be addressed. CD45 isoform switching may also occur in other ILC subsets, as several recent mass cytometry studies have reported that the presence of CD45RO$^+$ ILC(-like) cells (*67*–*69*) and chronic stimulation of NKG2C$^+$ natural killer cells in vitro induced CD45RO expression (*70*). CD45 isoform switching may thus play a broader functionally important role in ILC biology.

Migratory iILC2s represent a major early source of type 2 cytokines and subsequent protection against helminth infections in mice (*18*, *20*). Mouse iILC2s can be distinguished from nILC2s by higher expression levels of KLRG1 and IL17RB, strongly reduced levels of intracellular arginase 1 (ARG1), and a unique dependency on the transcription factor BATF (*14*, *20*, *21*). Like iILC2, human CD45RO$^+$ ILC2s described here can enter the circulation, express KLRG1 and IL17RB, do not express ARG1, and appear to rely on BATF for their full activation by epithelial alarmins. Our comparisons of transcriptional hallmarks of the various ILC2 subsets revealed a strong similarity between human CD45RO$^+$ ILC2s and mouse iILC2s. Our findings strongly suggest that human CD45RO$^+$ ILC2s are functionally akin to the iILC2s described in mouse models of type 2 inflammation.

We envision several nonmutually exclusive scenarios for the accumulation of CD45RO$^+$ ILC2s in inflamed tissues and in the circulation of patients with asthma or CRSwNP. Tissue-resident CD45RA$^+$ ILC2s could act as a local reservoir for the rapid generation of CD45RO$^+$ ILC2s in response to epithelial alarmins. Subsequently, CD45RO$^+$ ILC2s migrate out of the inflamed tissues into the PB. This is consistent with a recent study of parasite-induced type 2 inflammation in mice, demonstrating that tissue-specific pathways extrude locally activated ILC2s into the circulation (*22*). Alternatively, CD45RO$^+$ ILC2s present within inflamed mucosal tissues could have migrated from other ILC2-rich sites such as adipose fat or the gut. This is in line with migration of mouse iILC2s from the intestine to the lung during helminth infection (*18*) and with previously suggested human ILC2 recruitment into the airways upon nasal challenges of patients with asthma or aspirin-exacerbated respiratory disease (*33*, *71*).

Our findings have important implications for understanding the role of ILC2s in human type 2 immunopathologies, such as asthma and CRSwNP. A significant number of patients respond poorly to corticosteroid therapy, which remains a critical challenge in clinical management and a major focus of research (*36*–*38*). Previous studies have investigated the sensitivity of ILC2s to steroids, often with conflicting results (*29*–*32*, *34*, *35*). A recent study has implicated IL-7α receptor (CD127) signaling via IL-7 or TSLP stimulation in conferring human ILC2s with enhanced steroid resistance (*32*). Our results show that efficient CD45RA-to-CD45RO conversion does not strictly rely on IL-7 or TSLP, as IL-2 and IL-33 are sufficient to generate highly steroid-resistant CD45RO$^+$ ILC2s. However, it should be noted that at least one STAT5-activating cytokine (i.e., IL-2, IL-7, or TSLP) was required for IL-33 (or IL-1β) to induce CD45RA-to-CD45RO ILC2 conversion in our assay, indicating that STAT5 is critical to generate CD45RO$^+$ ILC2s and for acquisition of steroid resistance. Differential steroid resistance of CD45RA$^+$ and CD45RO$^+$ ILC2 populations could reconcile findings from these earlier reports, because ILC2 populations obtained from different sources (e.g. PB versus NPs) can vary widely in their CD45RA$^+$-to-CD45RO$^+$ ratios.

This will critically affect the steroid sensitivity of isolated ILC2s in culture, which can be further influenced by in vitro exposure to activating cytokines. Hence, an accurate assessment of ILC2 steroid responsiveness should include careful determination of CD45 isoform status.

Dexamethasone suppresses proliferation and cytokine production in CD45RA$^+$ ILC2s exposed to activating cytokines, without inducing apoptosis. Unexpectedly, dexamethasone appears to achieve suppression of an inflammatory ILC2 phenotype not only by down-regulating the type 2 inflammatory program but also by the concomitant activation of an immunomodulatory gene set that includes strong induction of amphiregulin expression. Amphiregulin not only is a critical molecule for tissue repair (*8*) but also can promote pathogenic tissue remodeling characteristic for patients with CRSwNP and asthma (*72*, *73*). The effects of corticosteroids thus go beyond suppression of inflammatory cytokine production and include phenotypic skewing of effector cells. CD45RA$^+$ ILC2s exposed to a combination of activating signals and corticosteroids, a scenario likely to occur in patients, could differentiate into an ILC2 subset that promotes tissue repair rather than inflammation. This is in line with our transcriptome analysis of NP ILC2s, which contain CD45RA$^+$ ILC2s and express high levels of amphiregulin. Although beneficial for inhibiting the activation of CD45RA$^+$ ILC2s, a chronic exposure to corticosteroids and activating cytokines could skew these ILC2s to promote excessive tissue remodeling.

Once CD45RA$^+$ ILC2s are converted into CD45RO$^+$ cells, dexamethasone could no longer efficiently suppress proliferation and cytokine production. We excluded the down-regulation of GR expression as a mechanism of steroid resistance. Instead, our transcriptome analyses point toward metabolic reprogramming underlying the steroid resistance of CD45RO$^+$ ILC2s. We observed marked up-regulation of genes involved in metabolic detoxification pathways, most notably GST enzymes. Conjugation of glutathione to steroids and their subsequent elimination provides a plausible mechanism explaining the intrinsic steroid resistance of CD45RO$^+$ ILC2s (*61*). In support of this conclusion, activation of these metabolic pathways was not observed in steroid-sensitive CD4$^+$ T cells. The signals and transcription factors that activate this metabolic circuit selectively in ILC2s are unknown, although AP-1 family proteins play important roles in regulating the expression of GST genes (*74*). In this context, an ILC2-specific interplay between BATF and additional transcription factors could up-regulate GST gene expression in CD45RO$^+$ ILC2s to confer steroid resistance. Additional studies are required to further dissect the role of glutathione metabolism in steroid-refractory asthma and explore this pathway as a potential new therapeutic target.

Our findings directly link CD45RO$^+$ inflammatory ILC2s to type 2 immunopathology. Besides being abundantly present in inflamed mucosal tissue of patients with CRSwNP (~50% of the total ILC2 population is CD45RO$^+$), we also detected significant levels of CD45RO$^+$ ILC2s in PB samples from patients with CRSwNP and uncontrolled asthma (up to ~65%). In contrast, ILC2s from noninflamed nasal TB tissue or PB from healthy donors and controlled asthmatics showed only minor proportions of CD45RO$^+$ cells (~5 to 20%). On the basis of these data, we propose that the CD45 isoform expression profile of the circulating ILC2 compartment represents a biomarker for severe type 2 inflammation in tissues. Our data may also explain contradictory findings regarding the positive correlation between circulating ILC2 abundance and asthma, as we show that such a correlation is specific for CD45RO$^+$ ILC2s and only seen in patients with uncontrolled asthma or during exacerbations. Extending our findings to other inflammatory disorders with (possible) ILC2 involvement should be pursued in future studies.

In conclusion, we identify an inflammatory human ILC2 subset in mucosal tissue and PB specifically marked by expression of CD45RO. This inflammatory ILC2, akin to the previously identified mouse iILC2, is resistant to suppression by corticosteroids and elevated in patients suffering from severe CRSwNP or asthma. Hence, CD45RO$^+$ ILC2s may represent an important new therapeutic target for improving the treatment of type 2 respiratory diseases.

MATERIALS AND METHODS

Study design

The goal of this study was to use transcriptome and flow cytometry analyses to identify molecular features that separate resting from activated inflammatory ILC2s in humans. We used PB mononuclear cell (PBMC) fractions from HCs and patients with asthma (from a cohort of 62 patients), NPs from chronic rhinosinusitis patients, and noninflamed nasal TB tissue from HCs to isolate ILC2s from different tissue microenvironments. An in vitro culture system was used for validation and functional studies.

Participants

NPs were collected from patients with chronic rhinosinusitis undergoing endoscopic sinus surgery. Noninflamed nasal inferior TBs were obtained from patients that underwent corrective surgery for hypertrophy with or without septoplasty. Written informed consent was obtained in accordance with approved protocols by the Medical Ethical Committee of the Academic Medical Centre (Amsterdam) and the Erasmus MC (Rotterdam). Buffy coats were provided by the Sanquin Blood bank. Patients with asthma (aged 18 to 75) were recruited by the Franciscus Gasthuis and Vlietland hospital in Rotterdam. Smokers (>10 pack-years), obese patients (body mass index > 35), and patients who received systemic corticosteroid therapy 3 months before blood draw were excluded. Healthy age- and gender-matched individuals were recruited as controls. Cohort characteristics are shown in table S3. Patients with asthma filled in a standardized ACQ and were scored into the following groups: controlled (<0.75), partially controlled (0.75 to 1.5), and uncontrolled (>1.5) asthma (*54*). Patients were also subdivided into low (0 to 500 dose equivalent units), medium (500 to 1000 dose equivalent units), and high (>1000 dose equivalent units) inhaled steroid intake groups by converting their individual steroid dosage to dose equivalent units according to recently published guidelines (*75*). "Steroid-sensitive" patients were identified as those with low ACQ score (<0.75) regardless of their steroid dose, whereas "steroid-resistant" patients were identified as those with a high ACQ score (>1.5) in combination with high steroid dosage (>1000 dose equivalent units, see above). All participants provided a written informed consent, and all experimental procedures were reviewed and approved by the Medical Ethical Committees of the Franciscus Gasthuis and the Erasmus MC.

Isolation of cells

Nasal tissues were processed as previously described (*76*). PBMCs were isolated from buffy coats or asthma patient blood draws as previously described (*77*).

Flow cytometry analysis and sorting

To purify ILC2s for cultures, PBMCs from buffy coats were first depleted for lineage$^+$ cells (CD3, CD4, CD16, CD14, and CD19) by magnetic-activated cell sorting (MACS) using MojoSort streptavidin Nanobeads (BioLegend) and LD Columns (Miltenyi Biotec). After MACS, cells were rested overnight in RPMI 1640 medium supplemented with 5% fetal calf serum (FCS) at 4°C. The next morning, cells were extracellularly stained with antibodies for 30 min at 4°C and with LIVE/DEAD Fixable aqua for 15 min at 4°C. CD45RA$^+$ ILC2s were sorted by fluorescence-activated cell sorting (FACS) using FACSAria III (BD Biosciences). ILC2s were identified as lineage$^-$CD127$^+$CD56$^-$CRTH2$^+$ (lineage$^-$ defined as CD3, CD4, CD14, CD16, CD5, CD94, CD19, FCεRI, and TCRγδ negative; see fig. S1C for gating strategy), as recently described in detail (*76*). Table S4 lists antibodies to human proteins used for phenotyping and cell sorting. ILC2s were isolated from NP as described previously (*76*). For intracellular cytokine stainings, cells were stimulated with PMA (10 ng/ml; Sigma-Aldrich) and ionomycin (500 nM; Merck) in the presence of GolgiStop (BD Biosciences) for 3 hours at 37°C. Cells were fixed with paraformaldehyde (2%, 10 min, 4°C) and permeabilized with saponin (0.5%, 30 min at room temperature). For intracellular transcription factor staining, cells were fixed with the eBioscience Foxp3/Transcription Factor Fixation/Permeabilization Concentrate and Diluent as described by the manufacturer. To analyze cell proliferation, sorted CD45RA$^+$ ILC2s were incubated with carboxyfluorescein diacetate succinimidyl ester (CFSE) (Thermo Fisher Scientific, 50 μM) in phosphate-buffered saline (PBS) for 10 min at 37°C. An excess of RPMI with 10% FCS was added to block the reaction, and cells were washed twice with Yssel's medium (see below) before culture. Cells were analyzed after 4 days of culture. Cell survival upon dexamethasone treatment was measured by staining cells with annexin V–phycoerythrin (PE) and 7-aminoactinomycin D (7-AAD; BD Biosciences) according to the manufacturer's instructions. The volume of annexin V and 7-AAD added was lowered from 5 to 2.5 μl per well to adjust for the lower numbers of cells analyzed per well. For analysis by flow cytometry, data were acquired on an LSR II flow cytometer (BD Biosciences) or LSRFortessa (BD Biosciences) and analyzed with FlowJo software (Tree Star Inc., USA).

ILC2 cultures and analysis of cytokine production

Sorted ILC2s were cultured in Yssel's medium (made "in house," Erasmus MC, Rotterdam) (*78*) supplemented with 1% normal human serum. Cells (2000 to 5000) were stimulated for 3 to 7 days with combinations of IL-2 (10 U/ml), IL-7 (20 ng/ml), IL-25 (20 ng/ml), IL-33, TSLP, IL-4, IL-12, IL18, IL-23, TGFβ, and IL-1β (all 50 ng/ml, unless stated otherwise). When indicated, dexamethasone was added to the culture medium (10^{-5} to 10^{-9} M, Sigma-Aldrich), starting either at day 0 or after 7 days of prestimulation with the indicated cytokines. For AP-1 inhibition, the small-molecule inhibitor T-5224 (MedChemExpress) was added to the culture medium (20 μM) at day 0. For CD45 phosphatase inhibition, NQ301 (Sigma-Aldrich) was added to the culture medium (25 nM) at day 0. IL-5 (Thermo Fisher Scientific) and IL-13 (BioLegend) levels were measured in culture supernatants by enzyme-linked immunosorbent assay (ELISA), using the manufacturer's protocols. For single-cell cloning, single CD45RA$^+$ ILC2s were sorted in 96-well plates coated with ~3000 OP9-DL4 cells in Yssel's medium supplemented with 1% normal human serum. Individual ILC2s were stimulated either with IL-2 (5 U/ml) and IL-7 (10 ng/ml) or with IL-2 (5 U/ml), IL-33 (25 ng/ml), and TSLP (25 ng/ml). Cells were kept in culture for 21 days before phenotypic analysis as described above.

Quantitative PCR

RNA was isolated from sorted or cultured ILC2s using the RNeasy Micro Kit (Qiagen) according to the manufacturer's instructions. RNA was synthesized into complementary DNA using RevertAid H Minus Reverse Transcriptase and random hexamer primers in the presence of RiboLock RNase inhibitor (Thermo Fisher Scientific). For quantitative reverse transcription polymerase chain reaction (qRT-PCR) reactions, probes from the Universal ProbeLibrary Set (Roche Applied Science) and TaqMan Universal Master Mix were used (Applied Biosystems, Foster City, CA, USA). qRT-PCRs were performed using the Prism 7300 Sequence Detection System (Applied Biosystems).

Transcriptome analysis using microarrays

RNA was isolated from sorted or cultured ILC2s as previously described (*79*). Briefly, total RNA was isolated from sorted cells flash-frozen in PBS and stored at −80°C before RNA extraction. QIAzol Lysis Reagent (Qiagen) was added to the cells, and RNA was isolated and purified using the RNeasy Micro Kit (Qiagen). Total RNA was amplified using the GeneChip WT Pico Kit (Thermo Fisher Scientific), generating biotinylated sense-strand DNA targets. Labeled samples were hybridized to human Clariom D Pico arrays (Thermo Fisher Scientific). Washing and staining were performed with GeneChip Fluidics Station 450, and scanning was conducted using GeneChip Scanner 3000 (both Thermo Fisher Scientific). All cell populations were analyzed in triplicate; data analysis was performed in RStudio (v1.1.383). Raw data were normalized using the RMA algorithm implemented in the limma Bioconductor R package (*80*). Adjusted *P* values were calculated with a moderated *t* test corrected for multiple testing using the Benjamini-Hochberg method. Data were visualized using glimma and pheatmap R packages (*81*).

RNA sequencing and downstream analysis

RNA was isolated from sorted or cultured ILC2s using the RNeasy Micro Kit (Qiagen) according to the manufacturer's instructions. Library preparation, high-throughput sequencing, and read alignment were performed as previously described (*12*). Sample scaling and statistical analysis were performed using the R package DESeq2 (*82*); genes with >0.5 absolute $\log_2$ fold change and an adjusted $P < 0.1$ (Wald test) were considered differentially expressed. Standard reads per kilobase per million (RPKM) values (or $\log_2$-transformed) were used as an absolute measure of gene expression. Genes with average RPKM < 1 in both experimental groups compared were considered not expressed and excluded from downstream analysis. Principal components analysis was conducted using the prcomp() function in R (executed from R Studio v1.1.383). *K*-means clustering was performed using Past3 software (https://folk.uio.no/ohammer/past/). Heatmaps, including hierarchical clustering on gene expression values, were performed using Morpheus (https://software.broadinstitute.org/morpheus/). Pathway enrichment analysis on differentially expressed genes and summarizing enriched pathways into gene-based networks were performed using Metascape (*83*). GSEA was performed using GSEA software (version 4.0.3, https://gsea-msigdb.org/gsea/index.jsp) in GSEA Preranked mode with standard settings. As input, we used a list of differentially expressed genes between PB (CD45RA$^+$) and

PB + type 2 (CD45RO$^+$) ILC2s (adjusted $P < 0.1$) preranked on the basis of their $\log_2$ fold change (CD45RO$^+$-CD45RA$^+$). Sets of genes up-regulated in mouse iILC2s or nILC2s were constructed from previously published RNA-sequencing data for mesenteric lymph node ILC2s (GSE145289) and lung ILC2s (GSE104708). DESeq2 was used as described above to identify differentially expressed genes between iILC2s and nILC2s. RNA-sequencing data from human CD4$^+$ T cells activated in vitro using anti-CD3/CD28 antibodies (GSE73213) were downloaded and processed as described above.

ChIP-sequencing data analysis

H3K4Me2 chromatin immunoprecipitation (ChIP)–sequencing data from human ILC2s were obtained from the Gene Expression Omnibus (GSE98843). Data were processed as previously described (*12*) and parsed to HOMER software (*84*) for downstream analysis. H3K4Me2-enriched regions were identified using HOMER findPeaks with -region -size 1000 -minDist 2500 options. Peaks were assigned to their nearest gene using the annotatePeaks script. Pathway enrichment analysis on peak-associated gene lists was performed using Metascape. Overlapping and nonoverlapping regions/peaks between two samples were identified using HOMER mergePeaks (-d given option), requiring a minimal overlap of 1 base pair. Peaks showing differential enrichment (fold change > 4, cumulative Poisson $P < 0.0001$) were determined using HOMER getDifferentialPeaks (-F 4 option). Histograms of ChIP-sequencing signal were generated using the annotatePeaks script (size 5000 -hist 10 options). The HOMER findMotifsGenome script (-size 1000 -mask -len 6,8,10,12 -S 20 options) was used to search for known transcription factor binding motifs ($n = 255$) in differentially enriched H3K4Me2$^+$ regions.

Statistical analyses

Statistical significance was determined using a Mann-Whitney *U* or Kruskal-Wallis test with GraphPad Prism software (v8). Statistical analyses of transcriptome datasets are described above.

SUPPLEMENTARY MATERIALS

immunology.sciencemag.org/cgi/content/full/6/55/eabd3489/DC1

Fig. S1. Transcriptome analysis of human ILC2s from the circulation and a mucosal tissue microenvironment.

Fig. S2. In vitro differentiation of resting CD45RA$^+$ ILC2s into inflammatory CD45RO$^+$ ILC2s.

Fig. S3. ILC2 conversion into a CD45RO$^+$ inflammatory phenotype is associated with BATF and IRF4 transcription factor activity.

Fig. S4. Circulating CD45RO$^+$ ILC2 frequencies are increased in uncontrolled and steroid-resistant asthma.

Fig. S5. CD45RO$^+$ inflammatory ILC2s are resistant to suppression by corticosteroids.

Fig. S6. Phenotypic conversion of CD45RA$^+$ ILC2s by dexamethasone and mechanisms underlying steroid resistance of CD45RO$^+$ ILC2s.

Table S1. Differentially expressed genes between PB and NP ILC2s (Excel spreadsheet).

Table S2. Gene expression values for genes belonging to six transcription factor families across PB, NP, and PB + type 2 ILC2s (Excel spreadsheet).

Table S3. Asthma patient cohort characteristics.

Table S4. Antibodies used in this study.

Table S5. Raw data file (Excel spreadsheet).

View/request a protocol for this paper from *Bio-protocol*.

REFERENCES AND NOTES

1. C. M. Lloyd, R. J. Snelgrove, Type 2 immunity: Expanding our view. *Sci. Immunol.* **3**, eaat1604 (2018).
2. D. Artis, H. Spits, The biology of innate lymphoid cells. *Nature* **517**, 293–301 (2015).
3. C. S. Klose, D. Artis, Innate lymphoid cells as regulators of immunity, inflammation and tissue homeostasis. *Nat. Immunol.* **17**, 765–774 (2016).
4. E. Vivier, D. Artis, M. Colonna, A. Diefenbach, J. P. Di Santo, G. Eberl, S. Koyasu, R. M. Locksley, A. N. J. Mc Kenzie, R. E. Mebius, F. Powrie, H. Spits, Innate lymphoid cells: 10 years on. *Cell* **174**, 1054–1066 (2018).
5. N. A. Yudanin, F. Schmitz, A.-L. Flamar, J. J. C. Thome, E. T. Wojno, J. B. Moeller, M. Schirmer, I. J. Latorre, R. J. Xavier, D. L. Farber, L. A. Monticelli, D. Artis, Spatial and temporal mapping of human innate lymphoid cells reveals elements of tissue specificity. *Immunity* **50**, 505–519.e4 (2019).
6. M. Colonna, Innate lymphoid cells: Diversity, plasticity, and unique functions in immunity. *Immunity* **48**, 1104–1117 (2018).
7. H. Kabata, D. Artis, Neuro-immune crosstalk and allergic inflammation. *J. Clin. Invest.* **130**, 1475–1482 (2019).
8. L. A. Monticelli, G. F. Sonnenberg, M. C. Abt, T. Alenghat, C. G. K. Ziegler, T. A. Doering, J. M. Angelosanto, B. J. Laidlaw, C. Y. Yang, T. Sathaliyawala, M. Kubota, D. Turner, J. M. Diamond, A. W. Goldrath, D. L. Farber, R. G. Collman, E. J. Wherry, D. Artis, Innate lymphoid cells promote lung-tissue homeostasis after infection with influenza virus. *Nat. Immunol.* **12**, 1045–1054 (2011).
9. L. A. Monticelli, L. C. Osborne, M. Noti, S. V. Tran, D. M. W. Zaiss, D. Artis, IL-33 promotes an innate immune pathway of intestinal tissue protection dependent on amphiregulin–EGFR interactions. *Proc. Natl. Acad. Sci. U.S.A.* **112**, 10762–10767 (2015).
10. B. W. S. Li, R. Stadhouders, M. J. W. de Bruijn, M. Lukkes, D. M. J. M. Beerens, M. D. Brem, A. K. Jan, I. Bergen, H. Vroman, M. Kool, W. F. J. van IJcken, T. N. Rao, H. J. Fehling, R. W. Hendriks, Group 2 innate lymphoid cells exhibit a dynamic phenotype in allergic airway inflammation. *Front. Immunol.* **8**, 1684 (2017).
11. L. J. Entwistle, L. G. Gregory, R. A. Oliver, W. J. Branchett, F. Puttur, C. M. Lloyd, Pulmonary group 2 innate lymphoid cell phenotype is context specific: Determining the effect of strain, location, and stimuli. *Front. Immunol.* **10**, 3114 (2019).
12. R. Stadhouders, B. W. S. Li, M. J. W. de Bruijn, A. Gomez, T. N. Rao, H. J. Fehling, W. F. J. van IJcken, A. I. Lim, J. P. Di Santo, T. Graf, R. W. Hendriks, Epigenome analysis links gene regulatory elements in group 2 innate lymphocytes to asthma susceptibility. *J. Allergy Clin. Immunol.* **142**, 1793–1807 (2018).
13. R. R. Ricardo-Gonzalez, S. J. Van Dyken, C. Schneider, J. Lee, J. C. Nussbaum, H.-E. Liang, D. Vaka, W. L. Eckalbar, A. B. Molofsky, D. J. Erle, R. M. Locksley, Tissue signals imprint ILC2 identity with anticipatory function. *Nat. Immunol.* **19**, 1093–1099 (2018).
14. Y. Huang, L. Guo, J. Qiu, X. Chen, J. Hu-Li, U. Siebenlist, P. R. Williamson, J. F. Urban Jr., W. E. Paul, IL-25-responsive, lineage-negative KLRG1^{hi} cells are multipotential 'inflammatory' type 2 innate lymphoid cells. *Nat. Immunol.* **16**, 161–169 (2015).
15. S. M. Bal, K. Golebski, H. Spits, Plasticity of innate lymphoid cell subsets. *Nat. Rev. Immunol.* **20**, 552–565 (2020).
16. M. T. Stier, J. Zhang, K. Goleniewska, J. Y. Cephus, M. Rusznak, L. Wu, L. Van Kaer, B. Zhou, D. C. Newcomb, R. S. Peebles Jr., IL-33 promotes the egress of group 2 innate lymphoid cells from the bone marrow. *J. Exp. Med.* **215**, 263–281 (2018).
17. M. R. Karta, P. S. Rosenthal, A. Beppu, C. Y. Vuong, M. Miller, S. Das, R. C. Kurten, T. A. Doherty, D. H. Broide, β_2 integrins rather than β_1 integrins mediate *Alternaria*-induced group 2 innate lymphoid cell trafficking to the lung. *J. Allergy Clin. Immunol.* **141**, 329–338.e12 (2018).
18. Y. Huang, K. Mao, X. Chen, M.-A. Sun, T. Kawabe, W. Li, N. Usher, J. Zhu, J. F. Urban Jr., W. E. Paul, R. N. Germain, S1P-dependent interorgan trafficking of group 2 innate lymphoid cells supports host defense. *Science* **359**, 114–119 (2018).
19. E. E. Dutton, D. W. Gajdasik, C. Willis, R. Fiancette, E. L. Bishop, A. Camelo, M. A. Sleeman, M. Coccia, A. M. Didierlaurent, M. Tomura, F. Pilataxi, C. A. Morehouse, G. Carlesso, D. R. Withers, Peripheral lymph nodes contain migratory and resident innate lymphoid cell populations. *Sci. Immunol.* **4**, eaau8082 (2019).
20. M. M. Miller, P. S. Patel, K. Bao, T. Danhorn, B. P. O'Connor, R. L. Reinhardt, BATF acts as an essential regulator of IL-25–responsive migratory ILC2 cell fate and function. *Sci. Immunol.* **5**, eaay3994 (2020).
21. A.-L. Flamar, C. S. N. Klose, J. B. Moeller, T. Mahlakõiv, N. J. Bessman, W. Zhang, S. Moriyama, V. Stokic-Trtica, L. C. Ranking, G. G. Putzel, H.-R. Rodewald, Z. He, L. Chen, S. A. Lira, G. Karsenty, D. Artis, Interleukin-33 induces the enzyme tryptophan hydroxylase 1 to promote inflammatory group 2 innate lymphoid cell-mediated immunity. *Immunity* **52**, 606–619.e6 (2020).
22. R. R. Ricardo-Gonzalez, C. Schneider, C. Liao, J. Lee, H.-E. Liang, R. M. Locksley, Tissue-specific pathways extrude activated ILC2s to disseminate type 2 immunity. *J. Exp. Med.* **217**, e20191172 (2020).
23. K. Zhang, X. Xu, M. A. Pasha, C. W. Siebel, A. Costello, A. Haczku, K. M. Namara, T. Liang, J. Zhu, A. Bhandoola, I. Maillard, Q. Yang, Cutting edge: Notch signaling promotes the plasticity of group-2 innate lymphoid cells. *J. Immunol.* **198**, 1798–1803 (2017).
24. A. I. Lim, S. Lopez-Lastra, R. Stadhouders, F. Paul, A. Casrouge, N. Serafini, A. Puel, J. Bustamante, L. Surace, G. Masse-Ranson, E. David, H. Strick-Marchand, L. L. Bourhis, R. Cocchi, D. Topazio, P. Graziano, L. A. Muscarella, L. Rogge, X. Norel, J.-M. Sallenave, M. Allez, T. Graf, R. W. Hendriks, J.-L. Casanova, I. Amit, H. Yssel, J. P. Di Santo, Systemic human ILC precursors provide a substrate for tissue ILC differentiation. *Cell* **168**, 1086–1100.e10 (2017).

25. M. Nagasawa, B. A. Heesters, C. M. A. Kradolfer, L. Krabbendam, I. Martinez-Gonzalez, M. J. W. de Bruijn, K. Golebski, R. W. Hendriks, R. Stadhouders, H. Spits, S. M. Bal, KLRG1 and NKp46 discriminate subpopulations of human CD117^{+}CRTH2^{-} ILCs biased toward ILC2 or ILC3. *J. Exp. Med.* **216**, 1762–1776 (2019).
26. J. M. Mjösberg, S. Trifari, N. K. Crellin, C. P. Peters, C. M. van Drunen, B. Piet, W. J. Fokkens, T. Cupedo, H. Spits, Human IL-25- and IL-33-responsive type 2 innate lymphoid cells are defined by expression of CRTH2 and CD161. *Nat. Immunol.* **12**, 1055–1062 (2011).
27. I. K. Krohn, S. M. Bal, K. Golebski, The role of innate lymphoid cells in airway inflammation: Evolving paradigms. *Curr. Opin. Pulm. Med.* **24**, 11–17 (2018).
28. E. K. van der Ploeg, A. C. Mascaro, D. Huylebroeck, R. W. Hendriks, R. Stadhouders, Group 2 innate lymphoid cells in human respiratory disorders. *J. Innate Immun.* **12**, 47–62 (2020).
29. H. Kabata, K. Moro, K. Fukunaga, Y. Suzuki, J. Miyata, K. Masaki, T. Betsuyaku, S. Koyasu, K. Asano, Thymic stromal lymphopoietin induces corticosteroid resistance in natural helper cells during airway inflammation. *Nat. Commun.* **4**, 2675 (2013).
30. P. Nagakumar, F. Puttur, L. G. Gregory, L. Denney, L. Fleming, A. Bush, C. M. Lloyd, S. Saglani, Pulmonary type-2 innate lymphoid cells in paediatric severe asthma: Phenotype and response to steroids. *Eur. Respir. J.* **54**, 1801809 (2019).
31. H. H. Walford, S. J. Lund, R. E. Baum, A. A. White, C. M. Bergeron, J. Husseman, K. J. Bethel, D. R. Scott, N. Khorram, M. Miller, D. H. Broide, T. A. Doherty, Increased ILC2s in the eosinophilic nasal polyp endotype are associated with corticosteroid responsiveness. *Clin. Immunol.* **155**, 126–135 (2014).
32. S. C. Liu, M. Verma, L. Michalec, W. Liu, A. Sripada, D. Rollins, J. Good, Y. Ito, H. W. Chu, M. M. Gorska, R. J. Martin, R. Alam, Steroid resistance of airway type 2 innate lymphoid cells from patients with severe asthma: The role of thymic stromal lymphopoietin. *J. Allergy Clin. Immun.* **141**, 257–268.e6 (2018).
33. R. Chen, S. G. Smith, B. Salter, A. El-Gammal, J. P. Oliveria, C. Obminski, R. Watson, P. M. O'Byrne, G. M. Gauvreau, R. Sehmi, Allergen-induced increases in sputum levels of group 2 innate lymphoid cells in subjects with asthma. *Am. J. Respir. Crit. Care Med.* **196**, 700–712 (2017).
34. Y. Jia, X. Fang, X. Zhu, C. Bai, L. Zhu, M. Jin, X. Wang, M. Hu, R. Tang, Z. Chen, IL-13^{+} type 2 innate lymphoid cells correlate with asthma control status and treatment response. *Am. J. Respir. Cell Mol. Biol.* **55**, 675–683 (2016).
35. S. Castanhinha, R. Sherburn, S. Walker, A. Gupta, C. J. Bossley, J. Buckley, N. Ullmann, R. Grychtol, G. Campbell, M. Maglione, S. Koo, L. Fleming, L. Gregory, R. J. Snelgrove, A. Bush, C. M. Lloyd, S. Saglani, Pediatric severe asthma with fungal sensitization is mediated by steroid-resistant IL-33. *J. Allergy Clin. Immunol.* **136**, 312–322.e7 (2015).
36. P. J. Barnes, Corticosteroid resistance in patients with asthma and chronic obstructive pulmonary disease. *J. Allergy Clin. Immunol.* **131**, 636–645 (2013).
37. R. Wadhwa, K. Dua, I. M. Adcock, J. C. Horvat, R. Y. Kim, P. M. Hansbro, Cellular mechanisms underlying steroid-resistant asthma. *Eur. Respir. Rev.* **28**, 190096 (2019).
38. W. W. Stevens, R. P. Schleimer, R. C. Kern, Chronic rhinosinusitis with nasal polyps. *J. Allergy Clin. Immunol. Pract.* **4**, 565–572 (2016).
39. V. Konya, J. Mjosberg, Lipid mediators as regulators of human ILC2 function in allergic diseases. *Immunol. Lett.* **179**, 36–42 (2016).
40. C. Wilhelm, O. J. Harrison, V. Schmitt, M. Pelletier, S. P. Spencer, J. F. Urban Jr., M. Ploch, T. R. Ramalingam, R. M. Siegel, Y. Belkaid, Critical role of fatty acid metabolism in ILC2-mediated barrier protection during malnutrition and helminth infection. *J. Exp. Med.* **213**, 1409–1418 (2016).
41. C. Beuraud, V. Lombardi, S. Luce, S. Horiot, E. Naline, C. Neukirch, S. Airouche, T. Perchet, R. Golub, P. Devillier, S. Chollet-Martin, V. Baron-Bodo, E. Nony, M. Aubier, L. Mascarell, P. Moingeon, CCR10^{+}ILC2s withILC1-like properties exhibit a protective function in severe allergic asthma. *Allergy* **74**, 933–943 (2019).
42. M. L. Hermiston, Z. Xu, A. Weiss, CD45: A critical regulator of signaling thresholds in immune cells. *Annu. Rev. Immunol.* **21**, 107–137 (2003).
43. T. Hochdorfer, C. Winkler, K. Pardali, J. Mjosberg, Expression of c-Kit discriminates between two functionally distinct subsets of human type 2 innate lymphoid cells. *Eur. J. Immunol.* **49**, 884–893 (2019).
44. J. H. Bernink, Y. Ohne, M. B. M. Teunissen, J. Wang, J. Wu, L. Krabbendam, C. Guntermann, R. Volckmann, J. Koster, S. van Tol, I. Ramirez, Y. Shrestha, M. A. de Rie, H. Spits, X. R. Ros, A. A. Humbles, c-Kit-positive ILC2s exhibit an ILC3-like signature that may contribute to IL-17-mediated pathologies. *Nat. Immunol.* **20**, 992–1003 (2019).
45. S. M. Bal, J. H. Bernink, M. Nagasawa, J. Groot, M. M. Shikhagaie, K. Golebski, C. M. van Drunen, R. Lutter, R. E. Jonkers, P. Hombrink, M. Bruchard, J. Villaudy, J. M. Munneke, W. Fokkens, J. S. Erjefält, H. Spits, X. R. Ros, IL-1β, IL-4 and IL-12 control the fate of group 2 innate lymphoid cells in human airway inflammation in the lungs. *Nat. Immunol.* **17**, 636–645 (2016).
46. M. D. Perron, S. Chowdhury, I. Aubry, E. Purisima, M. L. Tremblay, H. U. Saragovi, Allosteric noncompetitive small molecule selective inhibitors of CD45 tyrosine phosphatase suppress T-cell receptor signals and inflammation in vivo. *Mol. Pharmacol.* **85**, 553–563 (2014).
47. N. Serafini, C. A. Vosshenrich, J. P. Di Santo, Transcriptional regulation of innate lymphoid cell fate. *Nat. Rev. Immunol.* **15**, 415–428 (2015).
48. K. Bao, T. Carr, J. Wu, W. Barclay, J. Jin, M. Ciofani, R. L. Reinhardt, BATF modulates the Th2 locus control region and regulates CD4^{+} T cell fate during antihelminth immunity. *J. Immunol.* **197**, 4371–4381 (2016).
49. B. C. Betz, K. L. Jordan-Williams, C. Wang, S. G. Kang, J. Liao, M. R. Logan, C. H. Kim, E. J. Taparowsky, BATF coordinates multiple aspects of B and T cell function required for normal antibody responses. *J. Exp. Med.* **207**, 933–942 (2010).
50. T. L. Murphy, R. Tussiwand, K. M. Murphy, Specificity through cooperation: BATF-IRF interactions control immune-regulatory networks. *Nat. Rev. Immunol.* **13**, 499–509 (2013).
51. N. Ye, Y. Ding, C. Wild, Q. Shen, J. Zhou, Small molecule inhibitors targeting activator protein 1 (AP-1). *J. Med. Chem.* **57**, 6930–6948 (2014).
52. S. Oberdoerffer, L. F. Moita, D. Neems, R. P. Freitas, N. Hacohen, A. Rao, Regulation of CD45 alternative splicing by heterogeneous ribonucleoprotein, hnRNPLL. *Science* **321**, 686–691 (2008).
53. E. Glasmacher, S. Agrawal, A. B. Chang, T. L. Murphy, W. Zeng, B. V. Lugt, A. A. Khan, M. Ciofani, C. J. Spooner, S. Rutz, J. Hackney, R. Nurieva, C. R. Escalante, W. Ouyang, D. R. Littman, K. M. Murphy, H. Singh, A genomic regulatory element that directs assembly and function of immune-specific AP-1–IRF complexes. *Science* **338**, 975–980 (2012).
54. E. F. Juniper, P. M. O'Byrne, G. H. Guyatt, P. J. Ferrie, D. R. King, Development and validation of a questionnaire to measure asthma control. *Eur. Respir. J.* **14**, 902–907 (1999).
55. J. Hoppstädter, A. J. Ammit, Role of dual-specificity phosphatase 1 in glucocorticoid-driven anti-inflammatory responses. *Front. Immunol.* **10**, 1446 (2019).
56. F. Y. Liew, J. P. Girard, H. R. Turnquist, Interleukin-33 in health and disease. *Nat. Rev. Immunol.* **16**, 676–689 (2016).
57. H. Hassan, S. Sakaguchi, M. Tenno, A. Kopf, N. Boucheron, A. C. Carpenter, T. Egawa, I. Taniuchi, W. Ellmeier, Cd8 enhancer E8I and Runx factors regulate CD8α expression in activated CD8^{+} T cells. *Proc. Natl. Acad. Sci. U.S.A.* **108**, 18330–18335 (2011).
58. B. Koh, M. M. Hufford, D. Pham, M. R. Olson, T. Wu, R. Jabeen, X. Sun, M. H. Kaplan, The ETS family transcription factors Etv5 and PU.1 function in parallel to promote Th9 cell development. *J. Immunol.* **197**, 2465–2472 (2016).
59. C. Miyamoto, S. Kojo, M. Yamashita, K. Moro, G. Lacaud, K. Shiroguchi, I. Taniuchi, T. Ebihara, Runx/Cbfβ complexes protect group 2 innate lymphoid cells from exhausted-like hyporesponsiveness during allergic airway inflammation. *Nat. Commun.* **10**, 447 (2019).
60. M. D. Buck, D. O'Sullivan, E. L. Pearce, T cell metabolism drives immunity. *J. Exp. Med.* **212**, 1345–1360 (2015).
61. D. M. Townsend, K. D. Tew, The role of glutathione-S-transferase in anti-cancer drug resistance. *Oncogene* **22**, 7369–7375 (2003).
62. J. Banuelos, N. Z. Lu, A gradient of glucocorticoid sensitivity among helper T cell cytokines. *Cytokine Growth Factor Rev.* **31**, 27–35 (2016).
63. S. A. LaMere, R. C. Thompson, H. K. Komori, A. Mark, D. R. Salomon, Promoter H3K4 methylation dynamically reinforces activation-induced pathways in human CD4 T cells. *Genes Immun.* **17**, 283–297 (2016).
64. J. Irie-Sasaki, T. Sasaki, W. Matsumoto, A. Opavsky, M. Cheng, G. Welstead, E. Griffiths, C. Krawczyk, C. D. Richardson, K. Aitken, N. Iscove, G. Koretzky, P. Johnson, P. Liu, D. M. Rothstein, J. M. Penninger, CD45 is a JAK phosphatase and negatively regulates cytokine receptor signalling. *Nature* **409**, 349–354 (2001).
65. J. H. Cho, H.-O. Kim, Y.-J. Ju, Y.-C. Kye, G.-W. Lee, S.-W. Lee, C.-H. Yun, N. Bottini, K. Webster, C. C. Goodnow, C. D. Surh, C. King, J. Sprent, CD45-mediated control of TCR tuning in naïve and memory CD8^{+} T cells. *Nat. Commun.* **7**, 13373 (2016).
66. I. Martinez-Gonzalez, L. Mathä, C. A. Steer, M. Ghaedi, G. F. T. Poon, F. Takei, Allergen-experienced group 2 innate lymphoid cells acquire memory-like properties and enhance allergic lung inflammation. *Immunity* **45**, 198–208 (2016).
67. N. Li, V. van Unen, T. Höllt, A. Thompson, J. van Bergen, N. Pezzotti, E. Eisemann, A. Vilanova, S. M. C. de Sousa Lopes, B. P. F. Lelieveldt, F. Koning, Mass cytometry reveals innate lymphoid cell differentiation pathways in the human fetal intestine. *J. Exp. Med.* **215**, 1383–1396 (2018).
68. F. Roan, T. A. Stoklasek, E. Whalen, J. A. Molitor, J. A. Bluestone, J. H. Buckner, S. F. Ziegler, Correction: CD4^{+} group 1 Innate Lymphoid Cells (ILC) form a functionally distinct ILC subset that is increased in systemic sclerosis. *J. Immunol.* **196**, 3966 (2016).
69. N. L. de Vries, V. van Unen, M. E. Ijsselsteijn, T. Abdelaal, R. van der Breggen, A. F. Sarasqueta, A. Mahfouz, K. C. M. J. Peeters, T. Höllt, B. P. F. Lelieveldt, F. Koning, N. F. C. C. de Miranda, High-dimensional cytometric analysis of colorectal cancer reveals novel mediators of antitumour immunity. *Gut* **69**, 691–703 (2020).
70. A. Merino, B. Zhang, P. Dougherty, X. Luo, J. Wang, B. R. Blazar, J. S. Miller, F. Cichocki, Chronic stimulation drives human NK cell dysfunction and epigenetic reprograming. *J. Clin. Invest.* **130**, 3770–3785 (2019).
71. J. J. Eastman, K. J. Cavagnero, A. S. Deconde, A. S. Kim, M. R. Karta, D. H. Broide, B. L. Zuraw, A. A. White, S. C. Christiansen, T. A. Doherty, Group 2 innate lymphoid cells are recruited to the nasal mucosa in patients with aspirin-exacerbated respiratory disease. *J. Allergy Clin. Immunol.* **140**, 101–108.e3 (2017).

72. Y. Morimoto, K. Hirahara, M. Kiuchi, T. Wada, T. Ichikawa, T. Kanno, M. Okano, K. Kokubo, A. Onodera, D. Sakurai, Y. Okamoto, T. Nakayama, Amphiregulin-producing pathogenic memory T helper 2 cells instruct eosinophils to secrete osteopontin and facilitate airway fibrosis. *Immunity* **49**, 134–150.e6 (2018).
73. Y. Enomoto, K. Orihara, T. Takamasu, A. Matsuda, Y. Gon, H. Saito, C. Ra, Y. Okayama, Tissue remodeling induced by hypersecreted epidermal growth factor and amphiregulin in the airway after an acute asthma attack. *J. Allergy Clin. Immunol.* **124**, 913–920.e7 (2009).
74. V. Daniel, Glutathione S-transferases: Gene structure and regulation of expression. *Crit. Rev. Biochem. Mol. Biol.* **28**, 173–207 (1993).
75. R. Beasley, J. Harper, G. Bird, I. Maijers, M. Weatherall, I. D. Pavord, Inhaled corticosteroid therapy in adult asthma. Time for a new therapeutic dose terminology. *Am. J. Respir. Crit. Care Med.* **199**, 1471–1477 (2019).
76. L. Krabbendam, M. Nagasawa, H. Spits, S. M. Bal, Isolation of human innate lymphoid cells. *Curr. Protoc. Immunol.* **122**, e55 (2018).
77. I. Tindemans, H. Vroman, M. Lukkes, M. van Nimwegen, M. J. W. de Bruijn, B. W. S. Li, A. Kleinjan, G. M. de Boer, G. A. Tramper-Stranders, M. Kool, G.-J. Braunstahl, R. W. Hendriks, Increased surface expression of NOTCH on memory T cells in peripheral blood from patients with asthma. *J. Allergy Clin. Immunol.* **143**, 769–771.e3 (2019).
78. H. Yssel, J. E. De Vries, M. Koken, W. Van Blitterswijk, H. Spits, Serum-free medium for generation and propagation of functional human cytotoxic and helper T cell clones. *J. Immunol. Methods* **72**, 219–227 (1984).
79. K. Golebski, X. R. Ros, M. Nagasawa, S. van Tol, B. A. Heesters, H. Aglmous, C. M. A. Kradolfer, M. M. Shikhagaie, S. Seys, P. W. Hellings, C. M. van Drunen, W. J. Fokkens, H. Spits, S. M. Bal, IL-1β, IL-23, and TGF-β drive plasticity of human ILC2s towards IL-17-producing ILCs in nasal inflammation. *Nat. Commun.* **10**, 2162 (2019).
80. M. E. Ritchie, B. Phipson, D. Wu, Y. Hu, C. W. Law, W. Shi, G. K. Smyth, limma powers differential expression analyses for RNA-sequencing and microarray studies. *Nucleic Acids Res.* **43**, e47 (2015).
81. S. Su, C. W. Law, C. Ah-Cann, M.-L. Asselin-Labat, M. E. Blewitt, M. E. Ritchie, Glimma: Interactive graphics for gene expression analysis. *Bioinformatics* **33**, 2050–2052 (2017).
82. M. I. Love, W. Huber, S. Anders, Moderated estimation of fold change and dispersion for RNA-seq data with DESeq2. *Genome Biol.* **15**, 550 (2014).
83. Y. Zhou, B. Zhou, L. Pache, M. Chang, A. H. Khodabakhshi, O. Tanaseichuk, C. Benner, S. K. Chanda, Metascape provides a biologist-oriented resource for the analysis of systems-level datasets. *Nat. Commun.* **10**, 1523 (2019).
84. S. Heinz, C. Benner, N. Spann, E. Bertolino, Y. C. Lin, P. Laslo, J. X. Cheng, C. Murre, H. Singh, C. K. Glass, Simple combinations of lineage-determining transcription factors prime cis-regulatory elements required for macrophage and B cell identities. *Mol. Cell* **38**, 576–589 (2010).

Acknowledgments: We thank M. Kool, H. Vroman, I. Tindemans, and B. W. S. Li for their assistance in setting up the asthma cohort studies. We thank M. Lukkes for help with PBMC isolations. **Funding:** This work is supported by the European Research Council to H.S. (ERC advanced grant 341038). I.M.-G. is supported by a Marie Curie Fellowship (EU project 798927—MAGIC). B.A.H. is supported by a Netherlands Organisation for Scientific Research Veni fellowship (91618032). G.A.T.-S. is supported by Dutch Lung Foundation grant 4.1.18.226 and SAB (Dutch Foundation for Asthma Prevention) grant 2017/004. R.W.H. is supported by Dutch Lung Foundation grants 3.2.12.067 and 4.1.18.226. R.S. is supported by a Netherlands Organisation for Scientific Research Veni fellowship (91617114), an Erasmus MC Fellowship, and a Dutch Lung Foundation Junior Investigator grant (4.2.19.041JO). S.M.B. is supported by a Dutch Lung Foundation fellowship (6.2.17.196JO). R.S. and D.H. are supported by extra funds from Erasmus MC awarded by its Executive Board in the context of novel investment plans for the Department of Cell Biology. **Author contributions:** Study conception and design: S.M.B., R.S., R.W.H., and H.S.; data acquisition: E.K.v.d.P., K.G., M.v.N., J.R.F., I.M.-G., C.M.A.K., S.v.T., B.P.S., M.J.W.d.B., G.M.d.B., G.A.T.-S., G.-J.B., W.F.J.v.I., A.P.N., C.M.v.D., W.J.F., D.H., and S.M.B.; analysis and interpretation of data: E.K.v.d.P., K.G., B.A.H., H.S., R.W.H., R.S., and S.M.B.; drafting of manuscript: E.K.v.d.P., H.S., R.W.H., R.S., and S.M.B.; critical revision: all authors. **Competing interests:** H.S. is a consultant for GSK, uniQure, and AIMM Therapeutics. G.-J.B. has received grant support and/or speaking fees from Novartis, Sanofi, GSK, AstraZeneca, ALK, Teva, and Chiesi. A.P.N. has served on an advisory board for Sanofi. **Data and materials availability:** Gene expression data have been deposited in the Gene Expression Omnibus (GEO) under accession numbers GSE150846 and GSE152130.

Submitted 16 June 2020
Accepted 23 December 2020
Published 29 January 2021
10.1126/sciimmunol.abd3489

Citation: E. K. van der Ploeg, K. Golebski, M. van Nimwegen, J. R. Fergusson, B. A. Heesters, I. Martinez-Gonzalez, C. M. A. Kradolfer, S. van Tol, B. P. Scicluna, M. J. W. de Bruijn, G. M. de Boer, G. A. Tramper-Stranders, G.-J. Braunstahl, W. F. J. van IJcken, A. P. Nagtegaal, C. M. van Drunen, W. J. Fokkens, D. Huylebroeck, H. Spits, R. W. Hendriks, R. Stadhouders, S. M. Bal, Steroid-resistant human inflammatory ILC2s are marked by CD45RO and elevated in type 2 respiratory diseases. *Sci. Immunol.* **6**, eabd3489 (2021).

Science Immunology

Steroid-resistant human inflammatory ILC2s are marked by CD45RO and elevated in type 2 respiratory diseases

Esmee K. van der PloegKorneliusz GolebskiMenno van NimwegenJoannah R. FergussonBalthasar A. HeestersItziar Martinez-GonzalezChantal M. A. KradolferSophie van TolBrendon P. SciclunaMarjolein J. W. de BruijnGeertje M. de BoerGerdien A. Tramper-StrandersGert-Jan BraunstahlWilfred F. J. van IJckenA. Paul NagtegaalCornelis M. van DrunenWytske J. FokkensDanny HuylebroeckHergen SpitsRudi W. HendriksRalph StadhoudersSuzanne M. Bal

Sci. Immunol., 6 (55), eabd3489. • DOI: 10.1126/sciimmunol.abd3489

Defiant ILC2s resist steroids

Group 2 innate lymphoid cells (ILC2s) contribute to the inflammation associated with human allergic airway diseases, including asthma and chronic rhinosinusitis. Corticosteroid drugs are used to manage type 2 respiratory diseases, but steroid resistance may arise in the course of therapy. By comparing ILC2s from inflamed nasal polyps with blood ILC2s from healthy controls, van der Ploeg *et al.* observed that enhanced cytokine expression by nasal polyp ILC2s and loss of steroid responsiveness were both associated with ILC2s becoming CD45RO rather than CD45RA like most resting ILC2s. Expression of the CD45RO isoform by inflammatory ILC2s in blood was increased in patients with asthma and correlated with more severe airway disease. CD45RO is a candidate biomarker for human inflammatory ILC2s that correlates with acquisition of steroid resistance.